Raman identification of pigments and opacifiers: Interest and limitation of multivariate analysis by comparison with solid state spectroscopical approach - I. Lead-tin and Naples Yellow

Jacques Burlot, Divine Vangu, Ludovic Bellot-Gurlet, Philippe Colomban

Received: 20 June 2023 | Revised: 5 September 2023 | Accepted: 7 September 2023

DOI: 10.1002/jrs.6600

SPECIAL ISSUE - RESEARCH ARTICLE

Journal of RAMAN SPECTROSCOPY WILEY

Raman identification of pigments and opacifiers: Interest and limitation of multivariate analysis by comparison with solid state spectroscopical approach—I. Lead-tin and Naples Yellow

Jacques Burlot | **Divine Vangu** | **Ludovic Bellot-Gurlet** | **Philippe Colomban**

Sorbonne Université, CNRS, de la Molécule aux Nano-objets: Réactivité, Interactions et Spectroscopies, MONARIS UMR8233, Paris, France

Correspondence
Philippe Colomban, Sorbonne Université, CNRS, de la Molécule aux Nano-objets: Réactivité, Interactions et Spectroscopies, MONARIS UMR8233, 4 Place Jussieu, Paris 75005, France.
Email: philippe.colomban@sorbonne-universite.fr

Funding information
French Agence Nationale de la Recherche, Grant/Award Number: EnamelFC project ANR-19-CE27-0019-02

Abstract

Lead-tin/Naples Yellow provides a bright yellow color often used in combination with a blue-colored glass to obtain a variety of green hues to decorate enameled glass, metalware, and ceramics. From the analysis of about hundreds of enameled objects from French and Chinese productions of the 18th century, we identify and compare the Raman signatures representative of these yellow pigments. For the first time, we propose several procedures that allow us to compare our data with those obtained from the literature on the spectra of synthesized pigments also characterized by XRD. A first approach is a reasoned analysis of the parameters obtained from the spectral decomposition carried out on spectra visually selected as the most different and the "purest." A second approach uses multivariate analyses with principal component analysis (PCA) or hierarchical clustering of the spectra and of the band parameters originating from a spectral decomposition. It appears that the precise identification of the phase from simple observation of the sole Raman signature may be unreliable when only main peaks are detected due to the large non-stoichiometry of the phases and the resulting similarity of the Raman signatures. PCA analysis of the total Raman spectra does not allow relevant classifications due to the strong contributions induced by the bands of the silicate matrix. However, the combination of a reasoned analysis of the Raman spectra with the PCA of spectroscopic parameters extracted from Raman spectral decomposition appears effective in categorizing the different pigments. From the results discussed, at least three types of Raman signatures are identified for each Sn- and Sb-based pigment and correlate with the type, the period, and the location of enamel production.

KEYWORDS
China, enamels, Europe, Naples yellow, pigment

1 | INTRODUCTION

In glass and ceramic production, the yellow colors of glass (amorphous silicate) can be obtained by different processes. In the simplest technique, based on the dissolution of ions in the silicate network (called *transparent colors*),[1] the yellow color is obtained with Fe^{3+} ions. The other way is to use a yellow pigment obtained by precipitation or addition of a crystalline phase to the glaze. This old technique used from ~1500 BC in Egypt and Mesopotamia[2–4] is then achieved by saturating a lead-based glaze glass with antimony to obtain the precipitation of $Pb_2Sb_2O_7$ (oxyplumboroméite, previously bindheimite, belonging to pyrochlore supergroup).[5] This yellow coloring agent was widely used by Roman glassmakers, who also used cassiterite (SnO_2) as an opacifier, and this way led to more complex compositions by incorporating tin and other metals ($Pb_2Sb_{2-x-y}Sn_xM_yO_7$) likely from internal reaction in the molten silicate.[6] Some ions having indeed several valences, the firing atmosphere will control the valence state of multivalent ions and the oxygen non-stoichiometry. The lead antimonate seems to have been gradually replaced by that of lead stannates during the first centuries AD, and the latter becomes mostly employed by the fourth century.[3] Because of the mention of the 16th century recipe in the famous book of Picolpasso and/or due to their large use in 18th century enameled ware including Capodimonte productions[7] as well as in Italian paintings,[3,8–10] these pigments are generally called "Naples yellows." From the end of 19th to middle of 20th century, uranyl ion first and then CdS replace them, and now, vanadium- or praseodymium-doped cassiterite, -zirconia, or -zircon pigments are only used in crockery production.[11,12]

The ancient yellow pigments are complex solid solutions based on lead and tin oxides, whose compositions depend on the time and place of production in relation to the raw materials and technologies used. The fine characterization of pigment structure is necessary for the identification of ancient technologies, and we are interested in characterizing non-invasively these pigments using Raman spectroscopy, which can be performed using mobile instruments. However, given the variety of neighboring phases that can form and the complex environments in which they are present (glazes where amorphous and crystalline phases coexist in various amounts to control the hue/decoration), the mere observation of the presence/absence of the dominant Raman bands in the spectroscopic signatures is not sufficient to obtain a clear identification of the crystalline phases. Furthermore, the intensity of the Raman peaks that could be associated to the pigment is highly variable, and in most of the case, only the strongest peaks can be visible. X-ray (micro)diffraction (XRD) is the alternative approach to characterize mineralogical structures, but to date, it is not readily available with a mobile instrument, especially when micron-sized analysis volumes are required. Furthermore, due to the low proportion of crystalline phases, without a strong focus of the X-ray beam, X-ray diffraction is expected to be insufficiently efficient. As non-invasive on-site analyses are mandatory for the study of masterpieces,[1,7,12–28] in this work, we attempt to refine the possibilities of identifying the different types of yellow pigments from the Raman spectrum alone obtained on the glazes. Finally, glasses and ceramics are prepared from natural raw materials—and not from "pure" chemical products—which induces the formation of non-stoichiometric phases that may exhibit structural distortions not found in the synthetic phases characterized in the literature, making structural identification/definition more difficult.

In order to better categorize the yellow pigments and the phases that can be associated with them, we will compare the Raman spectra from the literature in which yellow phases have been characterized both by Raman microspectroscopy and by X-ray diffraction with the different Raman signatures identified in our previous works[12,17,19–26] on several dozen of exceptional enameled objects produced in Europe or in China during the 17th and 18th centuries, analyzed on-site with mobile Raman set-up. We will compare the classifications obtained by the reasoned approach of solid-state chemistry analysis and a multivariate approach (principal component and hierarchical clustering) of different datasets: spectra in their entirety, of certain spectral intervals, or of parameters extracted from spectral decompositions. This approach is relatively new and has only been used to some extent in the study of the Raman signatures of stained glass windows recorded on-site with mobile Raman set-up.[29] Our goal is to go further in the development of "tools" for the classification of Raman signatures collected on-site in a non-invasive way and to use them to study the transfer of enameling technologies from Europe to China since the end of the 17th century (Kangxi reign, Qing Dynasty) conducted by the Jesuits hosted at the Qing Court.[30–36]

2 | BACKGROUND ON YELLOW SYNTHESIZED PIGMENTS

We first summarize the information extracted from the literature on the different types of lead-based yellow pigments that have been characterized to date. Table 1 summarizes the different phases previously identified by XRD analyses.[5,8,9,37-50] Different types of yellow lead stannates have been distinguished, with "pure" lead-tin yellow type I (Pb_2SnO_4)[44,45,51,52] (Table 1: unit-cell a ~ 0.87276–0.87371 nm for tetragonal (*P4₂/mbc*) group and a ~ 0.87288–0.87358 nm for orthorhombic [*Pbam*] group), and lead-tin yellow type II[51,52] ($PbSnO_3$ or $Pb_2Sn_2O_6$ with pyrochlore[53-55] or perovskite[56] structure) (Table 1: unit-cell a ~ 1.0695–1.07186 nm, cubic [*Fd-3 m*] system), which may contain additional silicon ($PbSn_{1-x}Si_xO_3$).[57] The lead-tin yellow type II has been detected in many vitreous material excavated from Roman sites dated from the first century BC.[6,58,59] Beyond the characterization provided by XRD, in most other studies, the pigment identification is only deduced from the detection by elemental analysis of tin, antimony, and other elements likely to enter the composition: zinc, iron, knowing that the presence of silicon is linked to the silicate matrix. Long ago, probably up to Renaissance, these phases were formed by precipitation during the cooling of molten enamels and not by prior synthesis of pure pigment powder, which was then added to the glassy silicate matrix.

All above mentioned phases are built with two sublattices, one based on Pb^{2+} (heavy) ions (hereafter called A ions) and a second based on covalent-bonded octahedron connected by corner or edge (hereafter called BO_6). Consequently, their Raman spectra show rather similar signature, a strong peak at low wavenumber arising from the T′ (translational) mode of Pb^{2+} ions and vibrational, bending and stretching modes of BO_6 tetrahedron at higher wavenumber. The differences between the spectra of compounds derived from these solid solutions will be subtle.

Pyrochlores belong to a large family of crystalline materials ($A_2B_2X_6Y$ general formula, a framework of corner shared BO_6 octahedron, the X site being partially occupied by an oxygen atom [or an OH^- group] and hence the common $A_2B_2X_7$ formula, e.g., $Pb_2Sb_2O_{7-\delta}$) with a rich variety of technologically important functional properties.[60] Perovskite family is larger (ABO_3 general formula, also a framework of corner shared octahedral, the A site being occupied by different M^{2+} ions, Pb^{2+} in our case, and with a non-stoichiometry of oxygen which is frequent) and are used in many applications (electronics, piezoelectric, energy production, etc.). These phases are very often formed together during synthesis, and the preparation of single phase ceramic is rather complex.[61] Both structures developed a diversity of possible structural transformations including iso-symmetric, reconstructive, and phase transitions of second order.[60,62–64] The structures are ideally cubic (Fd-3m), but distortions are common (e.g., rhombohedral, orthorhombic, and monoclinic), in particular depending on the synthesis temperature, non-stoichiometry, and orderings and involves changes of the Raman signature.[5,65–68] It has been established that partial substitution by alkaline ions is necessary to stabilize the pyrochlore $PbSb_2O_7$ phase.[69] Consequently, the composition of the glassy matrix in which the crystals form should control the structure of the pigment.

The Raman efficiency can be very different; for instance, ideal cubic perovskite does not have Raman spectrum, and its Raman signature arises from distorted domains.[66] The firing conditions may also lead to the formation of $PbSb_2O_6$, with a rhombohedral trirutile structure.[53] The homolog $CaSb_2O_6$ has been well known as an opacifier since Antiquity[70] as well as the more oxidized compound, the pyrochlore $CaSb_2O_7$. In the trirutile structure, the octahedra are connected by the edges to form crowns (lattice: ~0.0522 × 0.0501 nm), and the D_{3d} symmetry leads to numerous Raman lines. All these structures therefore have fairly similar Raman signatures, especially when only the most intense peaks are visible, and it is therefore difficult to make a phase assignment on simple visual criteria.

3 | EXPERIMENTAL

3.1 | Studied artifacts

The Raman data are those previously measured on yellow and green glazes of a corpus of European artifacts, such as watches with sophisticated enamel decoration that were almost exclusively produced in France (mid-17th to mid-18th century),[19] and French porcelains, mainly of soft-paste type (late 17th to mid-18th century).[17,22] They also include Chinese painted and *cloisonné* enamels on metal objects (late 17th to late 18th century, i.e., the Kangxi [1661–1722], Yongzheng [1722–1735], and Qianlong [1735–1796] reigns of the Qing Dynasty) and on porcelains assumed to have been made for the Emperor, some of which are also assumed to have been produced at the workshop of the Forbidden City (Zaobanchu, 造辦處, Beijing, named *huafalang* 畫琺瑯 or *falangcai* 琺瑯彩), or in the imperial kiln of Jingdezhen, named *yangcai* 洋彩.[20–23] Pieces that were produced specifically for export in official kilns (*waixiao ci* 外銷瓷) or in private kilns (armorial and *Chine de Commande* Export porcelains) are also considered.[12]

TABLE 1 Crystallographic information of the different Naples Yellow phases mentioned in the text

Formula	Name	Crystal system	Space group	Structure type	Unit-cell (nm)	Synthesis/natural specimen	Refs
$Pb_2Sb^V{}_2O_7$	Lead antimony oxide (Naples Yellow)	cubic	*Fd-3 m*	Pyrochlore	a ~ 1.0677 at 900°C	$PbCO_3$, Sb_2O_3; 500°C for 24 h; 750°C for 24 h; 900°C for 24 h	Brisse et al.[5]
					a ~ 1.0529	$PbAc_2.3H_2O$ + antimonic acid; 250°C for 7 h; 390°C for 62 h; 520°C for 11 h; 680°C for 32 h; 730°C for 20 h	Brisse et al.[5]
					a ~ 1.0426		(ICDD Card No. 781 549)[37]
					a ~ 1.0470	Pb_3O_4, Sb_2O_3; 900–1,000°C for 5 h	Clark et al.[38]
					a ~ 1.0394	Pb_3O_4, Sb_2O_3 (Pb:Sb = 0.8:1) + NaCl (10 wt%); 900°C	Rosi et al.[39]
	Lead antimony oxide (bindheimite)				a ~ 1.0440	Natural specimens from several areas around the World	(ICDD Card No. 731 737)[40]
					a ~ 1.0447	Natural specimen from Otjimbo East, S.W. Africa	Brisse et al.[5]
	Lead antimony oxide (oxyplumboroméite)				a ~ 1.03783	Natural specimen from Harstigen mine, Värmland, Sweden	Hålenius and Bosi[41]
$Pb_2Sb^VSn^{IV}O_{6.5}$/ $Pb_2Sb^V{}_{2-x}Sn^{IV}{}_xO_{7-x/2}$	Lead antimony tin oxide	cubic	*Fd-3 m*	Pyrochlore	a ~ 1.05645	PbO, SnO_2, Sb_2O_3 (Pb:Sn:Sb = 2:1:1); 680, 800, 900, 950, and 1,000°C	(ICDD Card No. 390 928)[42]
					a ~ 1.055	Pb_3O_4, Sb_2O_3, SnO_2 (Pb:Sb:Sn = 2:1.5:0.5) + NaCl (10 wt %); 800°C	Hradil et al.[9]
					a ~ 1.0560 and ~1.0500	$PbCO_3$, Sb_2S_3, SnO_2 (Pb:Sb:Sn = 2.2:1.33:0.67); 900°C	Rosi et al.[39]
$Pb_2Sb_{2-x-y}Sn_xSi_yO_7$	Lead antimony tin silicon oxide	cubic	*Fd-3 m*	Pyrochlore	Not determined		
Pb_2SnO_4	Lead-tin oxide (lead-tin yellow type I)	tetragonal	*P_42/mbc*		a ~ 0.87371	$PbCO_3$, SnO_2 (molar ratio = 2:1); 750°C for 1w and then 1,000°C for 1 h.	(ICDD Card No. 240 589)[43]
					a ~ 0.87288–0.87293		Gavvari et al.[44]
					a ~ 0.87276		Spahr et al.[45]
		orthorhombic	*Pbam*		a ~ 0.87328–0.87358		Gavvari et al.[44]
					a ~ 0.87288		Spahr et al.[45]

TABLE 1 (Continued)

Formula	Name	Crystal system	Space group	Structure type	Unit-cell (nm)	Synthesis/natural specimen	Refs
$PbSnO_3/PbSn_{1-x}Si_xO_3$	Lead-tin oxide/Lead-tin silicon oxide (lead-tin yellow type II)	cubic	*Fd-3 m*		a ~ 1.0695	Pb_2SnO_4, SiO_2 (molar ratio = 3:2); 800–900°C	(ICDD Card No. 170 607)[46]
					a ~ 1.0715	Pb_3O_4, SnO_2, SiO_2 (Pb_2SnO_4: SiO_2 = 1:1); 900°C for 5 h	(ICDD Card No. 491 886)[38]
					a ~ 1.071	Pb_3O_4, SnO_2, SiO_2 (Pb:Sn:Si 6:3:[3–1]); 800–900°C	Dik et al.[8]
$Pb_2Sn_2O_6$	Lead-tin oxide	cubic	*Fd-3 m*		a ~ 1.071860		(ICDD Card No. 720 002)[47]
$Pb^{II}{}_2Sb^{V}{}_{2-x}Fe^{III}{}_xO_{7-X}$	Lead antimony iron oxide	cubic	*Fd-3 m*	Pyrochlore	a ~ 1.0483 for $Pb2Fe_{0.5}Sb_{1.5}O_{6.5}$	PbO, Fe_2O_3, Sb_2O_3 (Pb:Fe:Sb = 4:1:3); 680, 800, and 900°C	(ICDD Card No. 381 016)[48]
					a ~ 1.0441	Pb_3O_4, Sb_2O_3, Fe_2O_3 (Pb:Sb:Fe = 2:1.8:0.2); 900°C	Cartechini et al.[49]
					a ~ 1.048 for $Pb_2Sb_{1.7}Fe_{0.3}O_{6.7}$	PbO, Sb_2O_3, Fe_2O_3; 800°C for 16 h ×2	Alloteau et al.[50]
$Pb_2Sb_{2-x-y-z}Sn_xSi_yFe_zO_7$	Lead antimony iron silicon oxide	cubic	*Fd-3 m*	Pyrochlore			
$Pb^{II}{}_2Sb^{V}{}_{2-x}Zn^{III}{}_xO_{7-X}$	Lead antimony zinc oxide	cubic	*Fd-3 m*	Pyrochlore	a ~ 1.0496	Pb_3O_4, Sb_2O_3, ZnO (Pb:Sb:Zn = 2:1.5:0.5) + NaCl (10 wt %); 900°C	Rosi et al.[39]
					a ~ 1.0457	Pb_3O_4, Sb_2O_3, ZnO (Pb:Sb:Zn = 2:1.8:0.2); 900°C	Cartechini et al.[49]
$Pb_2Sb_{2-x-y-z}Sn_xSi_yZn_zO_7$	Lead antimony zinc silicon oxide	cubic	*Fd-3 m*	Pyrochlore			

3.2 | Raman spectra and fitting

The spectra used in this work were previously published[17,19–23] and recorded using a mobile Raman set-up consisting of a HE 532 spectrometer and its remote head SuperHead® (Horiba Scientific, Jobin-Yvon) equipped with either a 50X (NA = 0.45) Nikon or a 200X (NA = 0.62) Mitutoyo long working distance (of 17 and 13 mm, respectively) microscope objectives, and a Ventus Quantum frequency-doubled Nd:YAG laser of 300 mW. All elements are linked by optic fibers. The laser power at the sample ranges between 15 mW (colorless glaze) and 2 mW (dark colored enamel). Figure 1 shows the most representative spectra visually selected (a more complete set of representative spectra has been published in Colomban et al.[23]). The spectra selection criteria are a low intensity of the signature of the glassy silicate matrix (contribution of the broad vibration modes of SiO_4 around 500 and 1,000 cm^{-1}) and a low contribution of crystalline phases such as quartz and cassiterite, in order to obtain signatures that are as representative as possible of yellow pigments alone.

The spectra from the literature[39,49–51,71] presented in Figure 2 (see Table S1 for more information on the phases selected from the literature) were first converted into a picture in jpeg format from the original PDF of the articles with Able2Extract® (Version Professional 15.0) and then extracted with the WebPlotDigitizer® (Version 4.5) software available online in open access.[72] This second step involves loading the image of the spectra and then aligning and calibrating the axes corresponding to the Raman wavenumber (cm^{-1}) and the intensity. By selecting the color corresponding to that of the spectrum on the image, it is then possible to extract in .csv file format a large number of data points corresponding to the variables of the latter and thus to save the spectrum in .txt format usable on Raman spectroscopy software.

Whether for the spectra of our studies or those obtained from the literature, a linear segment baseline was subtracted using Labspec® software (5.25.15, 2007, Horiba Jobin-Yvon[73,74]), and the spectra were then decomposed into a sum of elementary bands using Peakfitting Origin® software (6.0, 1999, Microcalc Inc.). Lorentzian and Gaussian shapes were used for narrow and broad components, respectively.

3.3 | Multivariate analysis

After baseline correction (Figure 3A), the spectra from objects analyzed in the previous works were normalized with the online ChemFlow® (Version 20.05)[75] software following the Singular Normal Variate (SNV) transformation (Figure 3B).[76] The SNV transformation, method introduced by Barnes et al.,[77] sees each spectrum having its mean value subtracted and being then divided by its standard deviation, such as its new mean and standard deviation are 0 and 1, respectively. Principal component analyses (PCAs) are then performed, again using ChemFlow®, with a calculation based on a maximum of 20 principal components. The first analysis is conducted on the full spectra (i.e., the variables are the intensities at each point in the spectrum), and then, others were carried out on selected restricted spectral ranges—100–1,200, 100–700, and 100–590 cm^{-1}—in order to progressively exclude phases not necessarily related to the compounds of the Naples Yellow pyrochlores and related pigments.

In a second step, PCAs were conducted using as variables the parameters characterizing the elementary bands assigned/related to the Naples Yellow pyrochlores (i.e., ~140, ~330, ~450, and ~510 cm^{-1}) obtained from the spectral decomposition procedure of our spectra and those from the literature (the values of the width [FWHM], area, and center of gravity of the peaks).

Some of the PCA analyses are performed on all samples (those considered as "references" and those studied considered as "unknowns") in order to perform the calculation and examine their groupings. Other PCA analyses are performed by differentiating the two sets of samples. A first PCA analysis is performed, taking into account only the spectra considered as "reference," in order to define the most discriminating/relevant space/plane of principal components. Without participating in the definition of the principal components, the samples studied are then projected onto this space of principal components defined by the "reference samples" in order to visualize their affinities with the reference samples.

4 | RESULTS

4.1 | Considering the variability of expected structures

The similarity of the pyrochlore, perovskite, and trirutile structures and of the compositions will be reflected in the Raman signatures recorded on enameled decoration. Let us consider the corresponding expected Raman signatures.

Due to the high polarizability of Pb^{2+} ions and their high mass, the strong peak(s) below 150 cm^{-1} correspond(s) to the translation mode (T') of the Pb^{2+} ions whatever the structure, and the comparison of spectra of pyrochlore phases with different amount of tin and antimony led Vandenborre and Husson[54,55] to assign

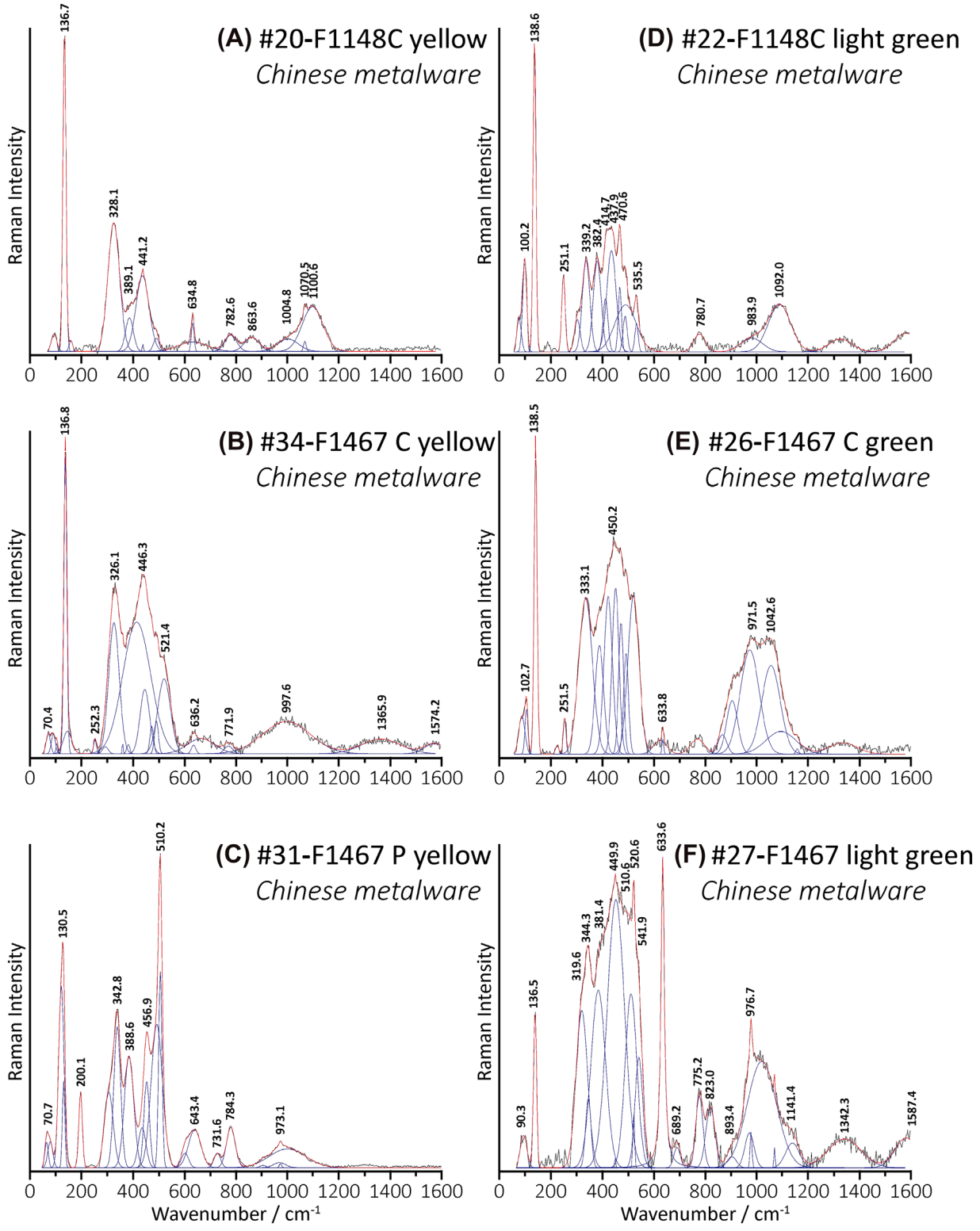

FIGURE 1 Representative spectra of the different Raman signatures (A to F; see the supporting information, Table S2) obtained for yellow or green enamels with their decomposition into elementary bands. Spectral decompositions were performed after baseline subtraction and using a Lorentzian shape for narrow peaks, a Gaussian shape for wide peaks and minimizing the number of bands needed to fit the experimental spectrum.

peaks around ~400 and 500 cm^{-1} to the internal modes involving Sn-O and Sb-O bonds, respectively, using calculations and atom substitutions. This was confirmed by different experimental studies of colored enamels[78] (Figure 1). It has also been shown that the position of the peak T′ depends on the firing temperature.[79,80] This can

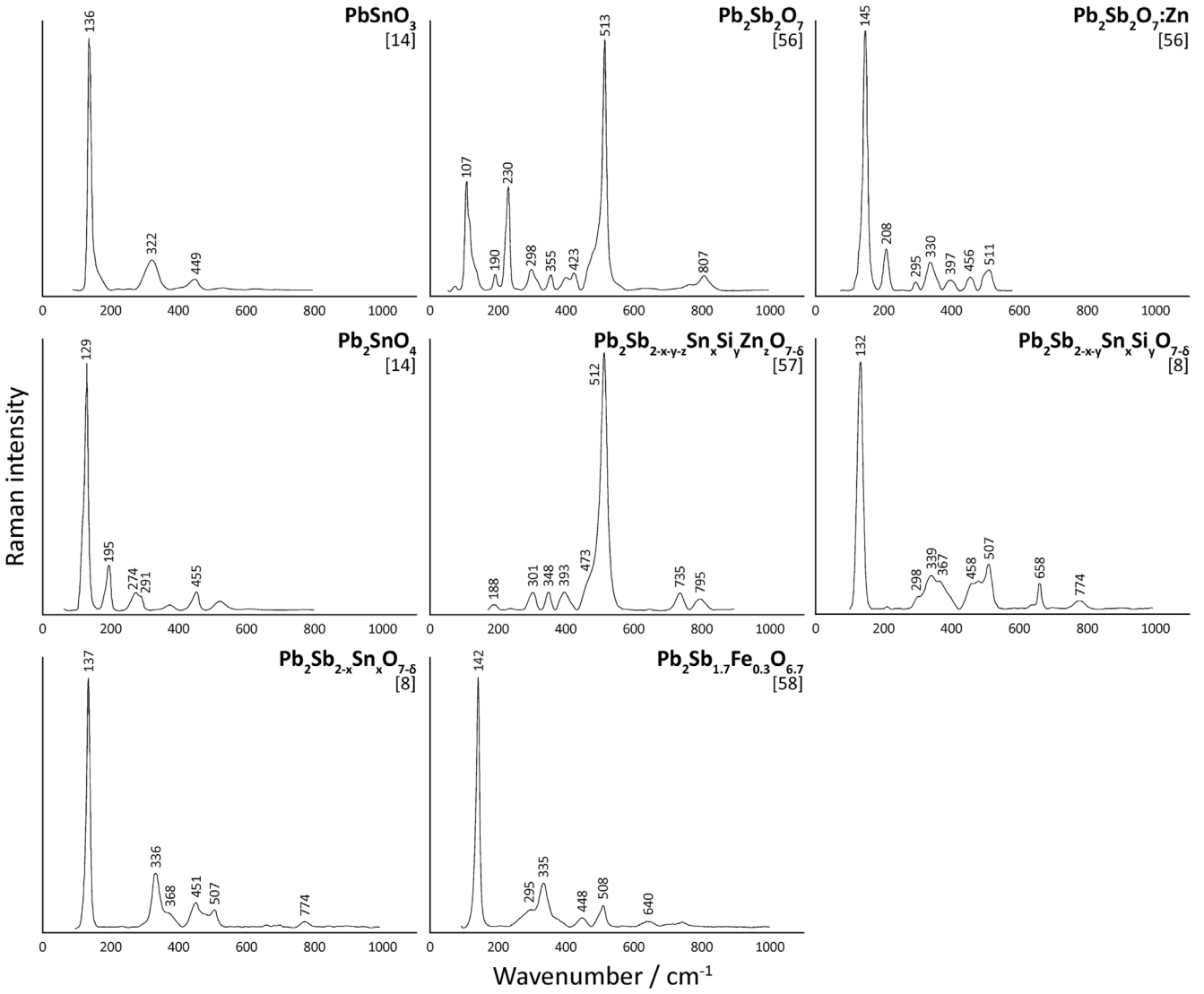

FIGURE 2 Selection of spectra from literature representative of the different mineral phases studied (yellow pigments).

be understood because the pyrochlore (as perovskite) phases undergo phase changes that shift the lattice modes. The firing of these glazes and its impact on the kiln atmosphere lead to changes in the $O_2/CO/CO_2$ balances, and therefore, the speciation of multivalent elements, such as Sb, can be changed and the structure distorted. Thus, as noted by Mihailova et al.[81] "as for perovskites, the factor group analysis can hardly explain the spectral behaviour of the phase." This behavior is general for structures composed of several vibrationally independent sub-lattices due to the mass contrast and/or the type of chemical bonds (here ionic/covalent).[82] The ion lattice is sensitive to the symmetry group seen by X-ray diffraction, while the covalent entities are more sensitive to site symmetry. The Raman signature will be thus sensitive to partial substitution and vacancies. This is both an advantage, since a spectrum will be a fingerprint of a given composition and firing process, in other words, the fingerprint of a workshop, and a drawback in deducing from Raman spectra a detailed description of the structural characteristics of mineral phases.

A cubic perovskite structure does not have an active Raman signature,[83,84] and the observed spectrum is weak and due to local regions where the chemical heterogeneity (i.e., the local non-stoichiometry) induces a structural distortion that exhibits a first order Raman spectrum[65,66]; the intensity of the resulting signal measures the extent of the distortion. The spectrum of perovskite phases is very broad, except for low wavenumber translation/lattice modes, which can be better defined. The presence of such phases is likely to be poorly detected in a composite material, especially using mobile Raman set-up.

For the cubic pyrochlore, factor group analysis[85–87] of $A_2B_2X_7$ predicts six Raman active modes:

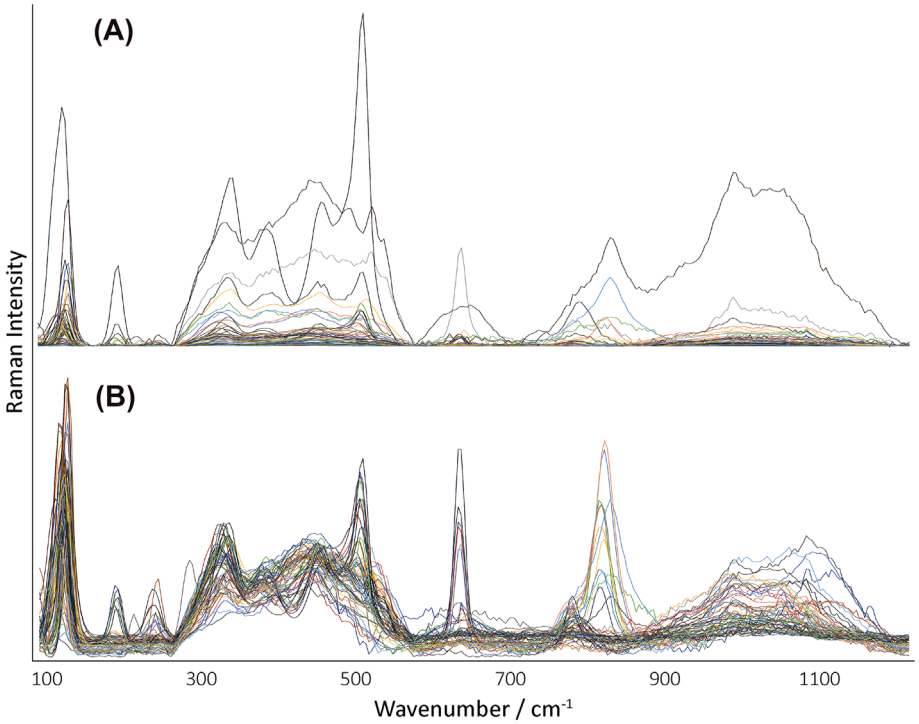

FIGURE 3 Raman spectra of the studied objects (56 different spectra): (A) after baseline subtraction; (B) then after Singular Normal Variate (SNV) transformation.

$$\Gamma = A_{1g} + E_g + 4F_{2g}$$

and seven F_{1u} active IR modes. Some IR modes can be Raman active due to the local disorder.[86] With the partial substitution, as for perovskite, each local (e.g., tin-based or antimony-based) domain will contribute, and hence, the number of active modes will be increased. Stress induced by the amorphous matrix may also give phase transition and new modes. As usual, Raman A_{1g} mode is expected strong and can be roughly described as a motion of oxygen atom of corner sharing octahedron coupled with some tilting mode.[88] It will appear at relatively high wavenumbers, as expected for M-O stretching mode in which oxygen atom motion is important. This is consistent with assignment of the ~450 and 510 cm^{-1} bands to Sn-O and Sb-O bond modes.

Factor group analysis of trirutile structure ($A_2B_2O_6$ tetragonal) also led to a much higher number of Raman active modes.[89]

The spectra of Figure 1A,B as well that of Figure 2 "$PbSnO_3$" correspond well to that expected for a pure cubic pyrochlore. However, in Figure 2, the rather broad modes above 150 cm^{-1} for $PbSnO_3$ indicate a disorder for the covalent/oxygen sub-lattice and the formula of the corresponding phase should be closer to $Pb_2Sn_2O_{6+\delta}$ than to $PbSnO_3$. The observation of a Raman spectrum exhibiting a high number of modes could indicate the presence of two or more phases with different compositions (that can coexist in a single grain as sub-domains) or even different distortions in relation with thermal history, stress, or (local) composition heterogeneity. We expect that perovskite phase cannot be detected by Raman scattering when mixed with pyrochlore phase due to the poor intensity of perovskite spectrum with a cubic or close to cubic structure.

4.2 | Considering the experimental variability of Raman signatures

Figure 1 summarizes all the different types of Raman signatures observed in the series of yellow or green enamels, where the green color is obtained by the dispersion of yellow pigment in an glassy matrix colored by Co^{2+} ions.[90] Despite the use of high magnification optics, generally 50X and even 200X in some cases, that is, focusing on volumes of the order of several μm^3 to about one μm^3, respectively, the contribution of the Raman signature of the silicate matrix can remain notable (underlined by deformation modes of the SiO_4 tetrahedron around 500 cm^{-1}, stretching mode around 1,000 cm^{-1}, and libration and translation/boson peak modes below 250 cm^{-1}).[13,91,92] This result suggests that, in some cases, the size of the pigment grains can be in the micrometer range, below the volume analyzed. The types of pigment spectra are distinguished by considering the position of the most intense peak, which either varies between 126 and 139 cm^{-1} or between 505 and 510 cm^{-1}, the presence of a peak around 90–100 cm^{-1}, a doublet well defined at ~330 and 440 cm^{-1}, and the possible presence

of peaks around 200 or 250 cm^{-1}. Note that, in the literature, the low wavenumber range, below 150 cm^{-1}, is not always measured (e.g., Figure 2, Sn-Sb-Si-Zn pigment). For some spectra, other phases may also be present, as quartz (main peak around 464 cm^{-1}, a residue of raw materials, not dissolved), cassiterite (doublet at 633 and 775 cm^{-1}, an opacifier), wollastonite (peak at 975 cm^{-1}, a phase formed when high calcium content led to precipitation of this phase), and lead (calcium/potassium) arsenate (peak at ~810–820 cm^{-1}, an opacifier). The later phases will be discussed in a companion paper in this special issue volume.[93]

On the basis of observations of the variability of the spectra visible to the eye, initial parameters are proposed for the classification of the spectra using binary diagrams representing the wavenumber of the strongest low wavenumbers peak (T'_{Pb} mode) and the area ratio of the ~510 cm^{-1} peak ($\nu_{Sb\text{-}O}$ mode) to that at ~130 cm^{-1}. The Figure 4 shows three groups of pigments, those for which there is no identifiable narrow peak around 500–510 (Group 1, assigned previously to pure lead-tin yellow[55]), those for which this peak is the stronger (Group 3, assigned previously to antimony-rich yellow[55]), and the others (Group 2, assigned previously to mixed compositions[55]) for which the fine peaks around 130 and 510 cm^{-1} are both observed. It should be kept in mind that to have a spectrum that is not dominated by the contribution of the spectrum of the silicate matrix, a very local analysis is required (high magnification objective) to collect the spectrum mainly corresponding to a grain of pigment. The relative intensity of the peaks then may also depend on the orientation of the grain with respect to the polarization of the laser beam, which could contribute to uncertainty on the horizontal axis of Figure 4. When information is available for elemental composition,[19–21] Group 1 indeed correspond to lead-tin yellow, and Groups 2 and 3 to complex compositions with antimony. Subgroups can be identified, for example, in Group 2. This one presents a greater variety for the ancient sample where pigments are embedded in an amorphous silicate matrix than for the pigments synthesized alone, without a matrix. For ancient samples (Figure 4A), the separation between Groups 1 and 2 is clearer than for reference samples.

Examination of the reference samples reported in Figure 2 confirms that Group 3 corresponds to compositions rich in antimony (Figure 4B). It is tempting, considering Figure 2, to associate subgroup 1, which has a band centered around 129 cm^{-1}, with "Pb_2SnO_4," and to associate the other sub-group, that is, centered at 136 cm^{-1} with "$PbSnO_3$." Recent work shows that Pb_2SnO_4 is characterized by an intense peak at 80 cm^{-1} outside the limit of the spectral windows of spectrometers commonly used for the study of Cultural Heritage artifacts.[45] The diversity of the spectra in Figure 2 for the antimony-containing phases is consistent with the broad areas defined for Groups 2 and 3.

4.3 | PCA conducted on the global Raman spectrum

Figure 3 clearly shows one of the difficulties in the Raman identification of pigments embedded in a glassy matrix, namely, the great variability of the relative contributions of the vitreous silicate matrix (broad bands at 500 and 1,000 cm^{-1}) on which the signature of the crystalline phases ("narrow" peaks) is superimposed.

The PCA conducted on the global spectra was performed over the 100–1,200 cm^{-1} interval (Figure 5). The comparison of the first and second component—being, respectively, 29.4% and 20.7% of the total variance, as shown in Figure 5—seems to isolate a group of 10 samples from the rest of the corpus. These 10 samples (all from Chinese workshops) are distinguished mainly by the fact that the Raman signatures feature the greatest intensities for the peak at ~820 cm^{-1} characteristic of the As-O bond,[94] associated with a shoulder at around ~775 cm^{-1}, which refer to the presence of opacifier, a form of arsenic apatite ($Na_{1-x-2y}K_xCa_yPb_4[AsO_4]_3$).[12,94] The two samples #53-R957-green and #32-F1467-green (see Table S2 for precise description of the studied artifacts), which are isolated from the rest of the corpus on Figure 5, also present this peak at ~820 cm^{-1}, but the latter being broader. This is tentatively assigned to the presence of another lead arsenate phase or to the very small size of the disordered apatite phase. The three samples grouped together in the lower right part of the diagram—#5-OA7074-green, #7-OA8338-yellow, and #21-F1448C-yellow—have Raman signatures clearly distinguishable from the others by combining, among others, both the peak at ~820 cm^{-1} and those at ~630 cm^{-1} characteristic of cassiterite. Thus, the PCA conducted over this wide range of wavenumbers does not provide any relevant information, as the highlighted groupings can be observed directly on the spectra and are not related to the characteristics of the yellow pigments. In any case, with this data processing, it is not possible to differentiate groups on the basis of information linked to the yellow pigments or even to the silicate matrix. It is the information linked to the opacifiers that mainly determine the groups underlined in Figure 5.

It is obvious that the variability of the contributions of the crystalline phases (pigments, residues, and opacifiers) and of the amorphous matrix do not allow the study of a particular pigment, as they cause a large variance in

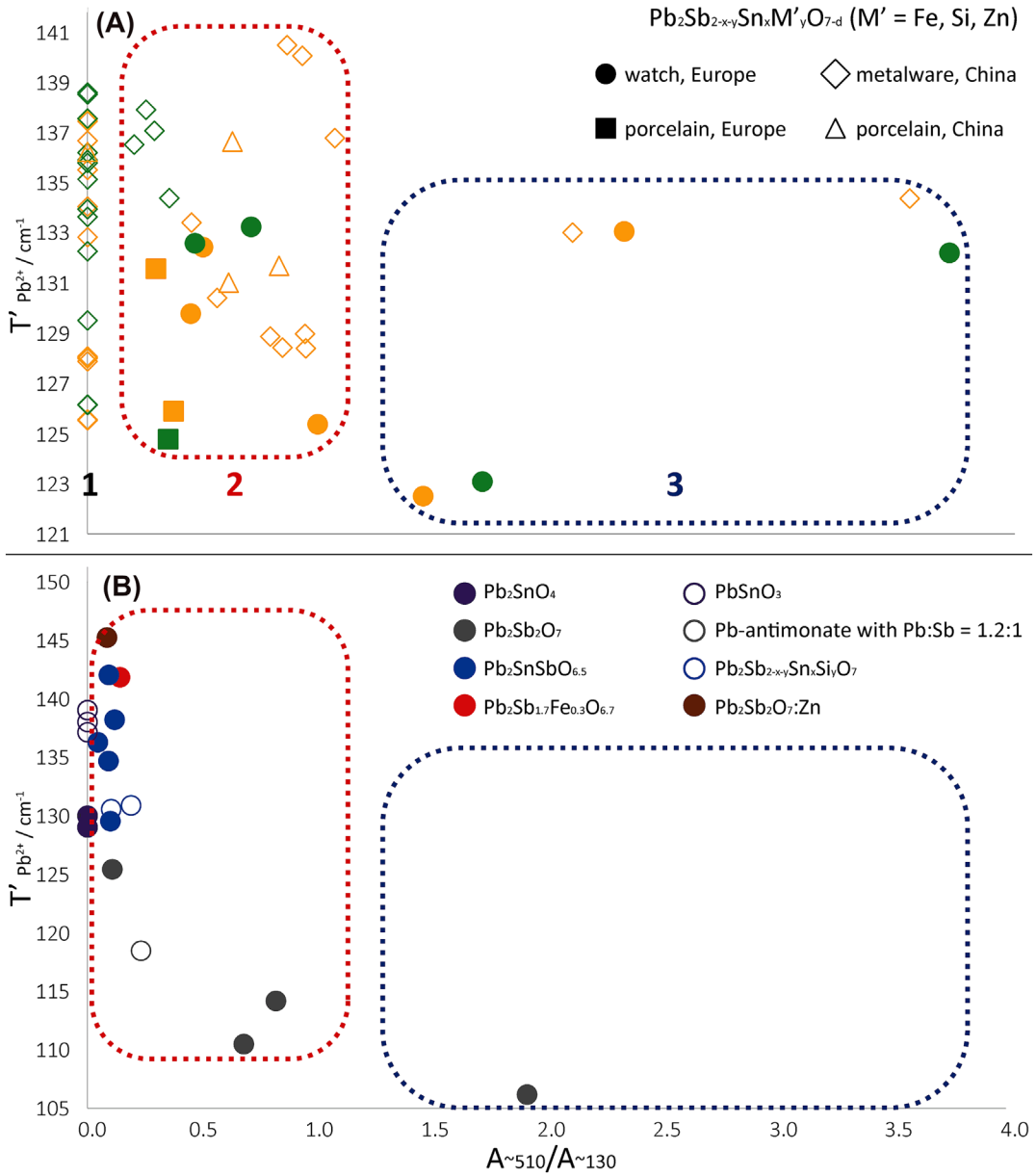

FIGURE 4 Distribution plot of the values of the Raman shift of the principal peak (T' Pb^{2+}) around 130 cm^{-1} versus the area ratio of the peak at ~510 cm^{-1} (linked to the presence of antimony) to that at ~130 cm^{-1}: (A) studied samples; (B) "references phases" from literature.

the spectra. This is particularly the case for painted enamels in which the mixtures of different pigments are made at sub-millimeter scales, even of the order of the micron as has been shown.[20,23–25,95]

4.4 | PCA conducted on selected spectral windows

We therefore looked at whether a stricter selection of the spectral window used, defined by excluding the regions where the "parasitic" phases give intense peaks, would allow a more efficient discrimination regarding the yellow pigments.

Thus, PCA were carried out over the 100–700 and the 100–590 cm^{-1} interval (Figures S1 and 6, respectively) to enable us to exclude the variance introduced by the main peak characteristic of As-O type structures, as well as those of the area of the stretching SiO_4 multiplets (900–1,100 cm^{-1}),[91] plus those of the main peak of cassiterite by considering the second, even more restricted, interval. In these configurations, it is the comparison of the second and the third principal component that was the most discriminating.

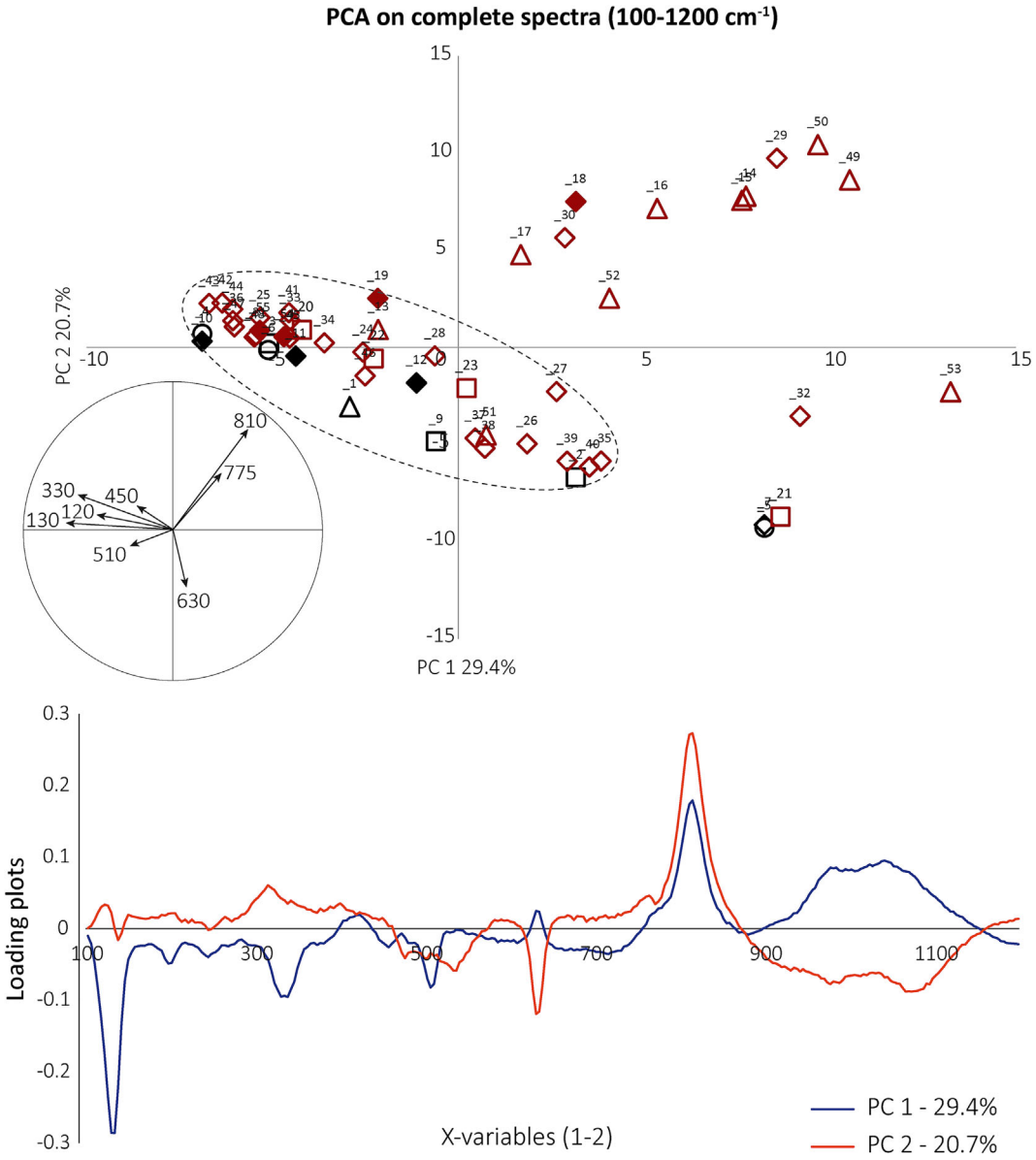

FIGURE 5 Diagram from PCA analysis with the first and second component calculated from the global (100–1,200 cm^{-1}) spectra of the corpus of studied objects and, below, the resulting loading plots showing the projection of PC 1 and 2 on the initial variable space. The inset circles represent the contributions on the principal component plane of some of the wavenumbers used in the PCA calculation.

In Figure 6, which shows the results of the PCA performed with the 100–590 cm^{-1} interval, three main groups of points stand out. The samples with negative loading values for the second component and positive values for the third one are, are those whose profiles of the peaks at ~330 and ~510 cm^{-1}, in particular, are the most marked in the sense that they are less influenced by the Raman signature of the massif corresponding to the SiO_4 bending mode of the silicate matrix. This group brings together all the European samples with the exception of #7-OA8338-yellow and #5-OA7074-green, as well as five Chinese samples, four of which can be detached from this group by their more isolated position on the diagram. These four samples have a very characteristic Raman signature with the presence of peaks around 130, 200, 340, 388, 450, and 510 cm^{-1}; a broad band centered at ~640 cm^{-1}; and a doublet at 726–780 cm^{-1}.

Thus, in the present case, what clearly differentiates these two groups of samples from the third main one is the ability to distinctly observe, or not, the peaks related to the pyrochlore phases within an interval of wavenumbers that can be "drowned out" by the peaks of the silicate network. It is interesting to note that the samples that clearly show these pigments-related peaks are mainly from European productions and seem to illustrate the use of complex Naples yellow pyrochlores that can be

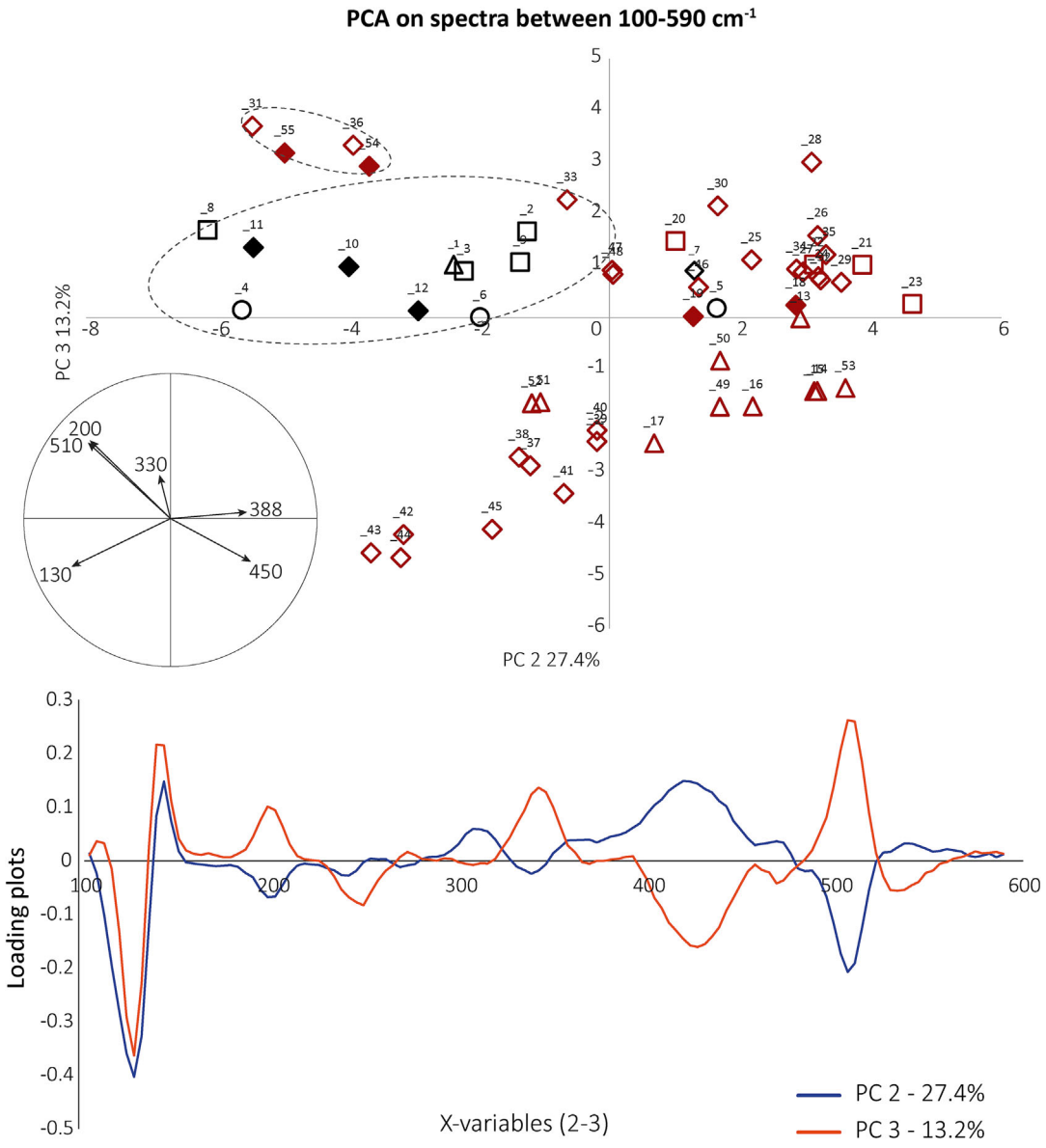

FIGURE 6 Diagram from PCA analysis with the second and the third component calculated from the spectra within the 100–590 cm^{-1} interval for the corpus of studied objects and, below, the resulting loading plots showing the projection of PC 2 and 3 on the initial variable space. The inset circles represent the contributions on the principal component plane of some of the wavenumbers used in the PCA calculation.

substituted with Zn and/or Sn for instance. In the case of samples whose glassy matrix is the most impactful in the Raman signatures, the PCA does not make it possible to differentiate them according to the nature of the pigment used.

For the PCA performed using the 100–700 cm^{-1} interval (Figure S1), which includes the influence of the main cassiterite peak at 630 cm^{-1}, it enables us to obtain the same groups of samples, but it separates less the group of the four "unique" signatures of samples #31-F1467-yellow, #36-F1467-yellow, #54-TH457-yellow, and #55-TH457-yellow. This PCA also isolates one sample—#7-OA8338-yellow—which is the only one for which the highest intensity peak in its Raman spectrum is the main representative of the cassiterite at 630 cm^{-1}. This sample has also the particularity of presenting one of the lowest intensities for the peak of the Pb-O bond of the pyrochlore phases centered around 140 cm^{-1}.

In short, the PCA conducted on spectral windows of the global spectra initially made it possible to separate the Raman signatures according to the presence/absence of the peak of the As-O bond in the 100–1,200 cm^{-1} interval and then to separate the samples distinctly presenting the association of the four peaks, ~340, ~388,

~450, and ~510 cm^{-1}, when we reduced the intervals up to 700 cm^{-1} and then 590 cm^{-1}. In these latter cases, the categorizations that could be made on the spectra were greatly influenced by the bulk of the peaks of the bending mode of the SiO_4 multiplets of the silicate matrix. By using this data treatment, it is not possible to classify the samples according to the nature of the pigment used but rather according to the pigment/vitreous matrix ratio. The discriminating aspect of this method remains interesting insofar, as it makes it relatively possible to separate European productions from Chinese ones. Indeed, since it is the signature of the silicate matrix that has the greatest impact on the definition of clusters in these PCAs, European lead-rich enamels stand out from Chinese lead-alkali ones.[17,19–23] In any case, the obtained classifications can be achieved by visual observation of the spectra without multivariate processing, which limits the interest in using PCAs without combining them with other processing or pre-processing of the data.

4.5 | PCA based on spectroscopic data extracted from spectral decomposition

4.5.1 | Samples selected as references

We now performed PCA on the data extracted from the spectral decomposition of the spectrum assigned to the pigment phase(s). Such an approach has already been used to discriminate between the different types of stained glass from their Raman spectra recorded on-site.[29] The variables used in the PCA are the center of gravity, the width, and the area of the characteristic peaks assigned to the Naples yellow family pigments, namely, those located around 120–140, 330, 450, and 510 cm^{-1}. Figure 7 shows the distribution of the phases presented in Figure 2, extracted from literature where phase characterization was made by XRD and Raman techniques, according to the first and second component calculated for the PCA.

We observe that the distribution of the phases representing the different types of yellow pigments is divided into four groups which are named A, A′, B, and C (+C′) (Figure 7). In the present case, the constitution of these groups results exclusively in the absence of one or several peaks used as variables, illustrating the sensitivity of the classification to variations in the spectral profiles associated with changes in structure/symmetry. Group A consists of the four samples of lead-tin yellow I (Pb_2SnO_4) whose Raman signatures show peaks at ~130 and ~450 cm^{-1}, and Group A′ concerns the other type of lead stannate pigment ($PbSnO_3$) featuring the two same peaks, plus those at ~330 cm^{-1}. We expect that the pigments of both groups have the pyrochlore structure and a true composition close to $Pb_2Sn_xO_{6-\delta}$, that is, with different speciation of tin. The samples of Group B seem to consist of the five samples of "pure" $Pb_2Sb_2O_7$ and the sample of mixed $Pb_2Sb_{2-x-y-z}Sn_xSi_yZn_zO_7$, a group that seems to be characterized by peaks at ~140 and ~510 cm^{-1} among the variables used. It seems from the literature that incorporation of silicon reduces distortion of the pyrochlore phase and promotes the cubic structure.[8] Group C is the one that contains the most "compounds." All the spectra found in this group present the four peaks, which explain why we find all the phases of lead antimonate doped with another metal, either Fe, Zn, or Sn. Only the lead antimonate sample, with a Pb:Sb ratio of 1.2:1 ($Pb_{1.1}Sb_{0.9}M_xO_{6.7+nx}$), constitutes Group C′. This sample features the peaks ~140, ~450, and ~510 cm^{-1}.

With the exception of the supposedly Si mixed compound (composition to be questioned?), the PCA carried out with the reference phases, and the parameters extracted from the decomposition of their Raman spectra separate perfectly according to the type of composition (stannate, antimonate and mixed) and structure/oxygen stoichiometry ($Pb_2Sn_xO_{6-\delta}$). As this classification is based on the number, position, and width of the Raman peaks that characterize the profiles of the Raman spectra, it highlights a reliable correlation with the structural symmetry.

4.5.2 | Corpus of yellow pigments in enamels studied

We use the space of principal components defined by the PCA carried out on the reference phases (Figure 7), and we project on it the parameters obtained from the decomposition of the Raman spectra collected on artifacts (Table S2). These samples therefore do not play a role in determining the classification presented in Figure 8.

Quite distinct from the others, one new group—D—and a sub-group B′ consisting solely of analyzed enamels samples were established. Because of their proximity, B′ appears to be a variant of B. It consists of one sample of European enamel on metal object and five enamel samples from Chinese metal objects. These eight samples of Group B′ feature the peaks at ~140, ~330, and ~510 cm^{-1}. The new group, named D, contains four samples of Chinese enamel on metal, all of green color, whose Raman signatures present the peaks at ~140 and ~330 cm^{-1}, but not at ~450 and ~510 cm^{-1} (Figure 9).

Groups A′ and C bring reference phases and enamel samples very close together. The enamels of Group A′ represent only samples from Chinese artifacts dated to the late 17th and 18th century. A total of 22 analyzed enamels are in this group: one enamel on porcelain and

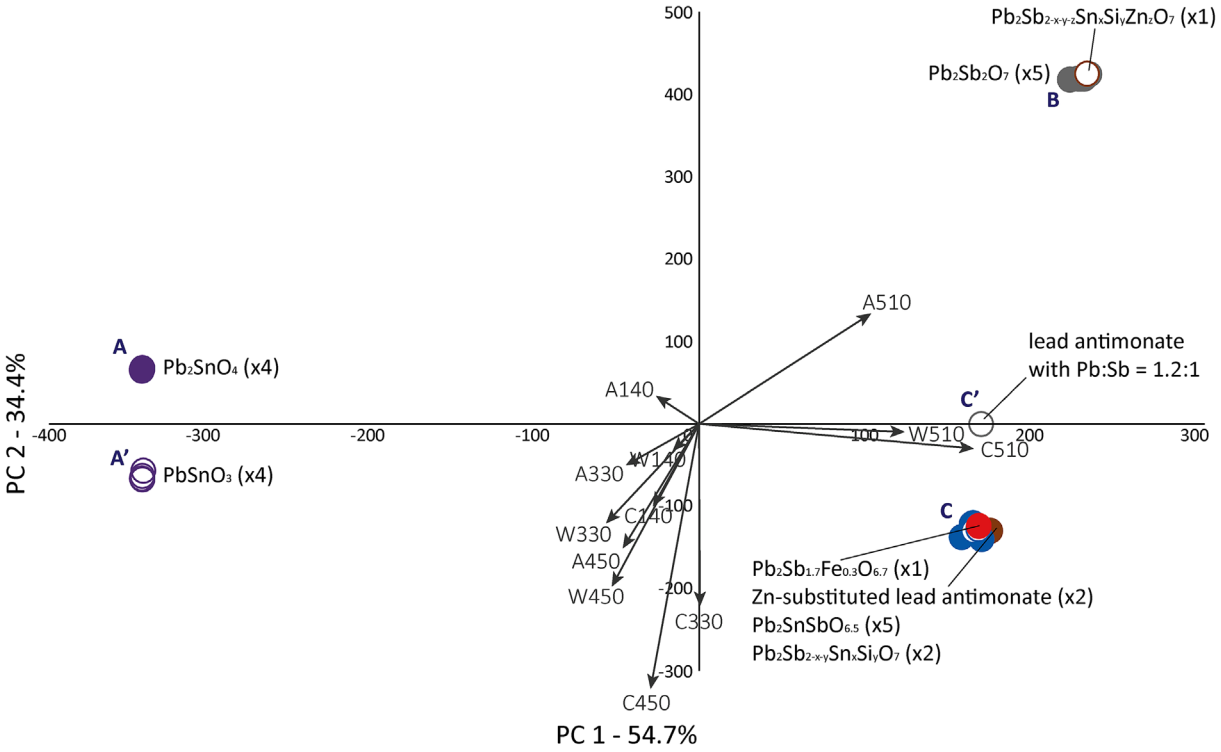

FIGURE 7 PCA diagram of the first and second components calculated from the corpus of spectra from the literature and the parameters extracted from their spectral decomposition (variables are the center of gravity [C], the width [W], and the area [A] of the peaks at ~140, 330, 450, and 510 cm^{-1}; centering option: yes; scaling option: no; number of PC max: 20). The vectors show the projection of the variables on the principal components plane. Variables grouped together are positively correlated, while variables positioned on opposite sides of the plot origin (the 510 vs. the 330 for example) are negatively correlated. The further a variable is from the origin, the more it contributes to the components of the factor plane.

21 enamels on metal objects. The Raman signatures of these samples show peaks at ~140, ~330, and ~450 cm^{-1}. Twenty-four enamel samples are present in Group C (Figure 8). Among these samples, 8 are European enamels on metal, 3 are European enamels on porcelain, 10 are Chinese enamels on metal, and 3 are Chinese enamels on porcelain. The signatures of these enamels, showing the four peaks used for the PCA variables, illustrate the use of a complex lead antimoniate pyrochlore that could have been be doped with Zn, Sn, or Fe for instance, likely with two different structures. However, based on our Raman measurements and data processing, it is not possible for us to define the composition of these pyrochlores more precisely.

5 | DISCUSSION

The distinction made empirically by visual examination of the spectra between three types of tin and antimony pyrochlores[19,78] is confirmed by the PCA performed using the parameters extracted from spectra decomposition and can be well illustrated too with the dendrogram obtained from hierarchical cluster analysis using the Euclidian distance and the Ward aggregation rule on the same variables extracted from the spectra decomposition (Figure 10).

For the antimony-rich phases, two groups are clear from hierarchical cluster analysis, those with the band at ~450 cm^{-1} (Figure 10: C and C′, lines red and orange) and those without (Figure 10: B and B′, lines green); for the tin-rich phases that do not show the band at ~510 cm^{-1}, they are characterized in particular by this relatively dominant band at 450 cm^{-1} (Figure 10: A and A′, lines blue and purple). Thus, three groups of signatures C, B, B′ and A′, A, and D′—are clearly identifiable in the analyzed objects for antimony and tin rich pigments (Figure 10: lines yellow), that is, one more than in the identification taking the literature spectra as references (Figure 7).

5.1 | Lead stannate yellow

The group characteristic of the Raman signature of the pigment lead-tin yellow I ($PbSnO_4$ according literature[44,45]) (Figure 7: Group A) does not contain any of our

studied enameled samples. On the contrary, Group A′, representative of the signature of lead-tin yellow II ($PbSnO_3$/$PbSn_{1-x-y}Si_xM_yO_3$), includes 22 enamel samples associated with the four references of this pigment (Figure 8). The criterion that differentiates the two types of lead stannate yellow, based on our variables, is the presence of the peak around 330 cm^{-1}. In reference spectra, this is observed in literature between 322 cm^{-1}[151] and 325 cm^{-1},[96] while it is reported between 316 and 333 cm^{-1} among enamels studied here.

There are several possible scenarios to explain the presence of lead-tin yellow II in enamels. Either this pigment was prepared in advance, then dispersed in the silicate powder before firing, and (partially) preserved from dissolving and re-precipitation (large grains are then expected) during firing. Either it was formed during cooling from the silicate melt oversaturated in certain elements and precipitated homogeneously in the silicate matrix[1,11,97,98]; small (i.e., submicron) grains being thus expected. Another possibility is that the craftsmen used a pigment of the lead-tin yellow I type introduced before firing, which, during firing, and due to the saturation of the enamel in certain elements allowing silicon to enter its structure, would have been "transformed" to form lead-tin yellow II. Thus, to know if it is type I or II, which was initially used by the craftsmen, we cannot suppose it, except if type II was measured in Raman microspectroscopy at very high magnification in order to detect different forms within grains. Indeed, the observation of the pure $PbSnO_3$ spectrum with a 100X or 200X objective indicates grains of a few microns or more in size, consistent with the use of a pre-prepared pigment and not nucleation-precipitation by saturation with lead and tin.[12] For the study of lead stannate yellow pigments used in studied enamels, the lack of distinction between $PbSnO_3$ and $PbSnO_4$ leads us to propose instead a formula like $Pb_2Sn^{IV}{}_xSn^{II}{}_YO_{6+\delta}$ with different speciation of tin, that is, a firing in (partially) reducing atmosphere.

It is interesting to note that the group of samples of enamels colored by (pure?) lead stannate represents only Chinese objects, almost exclusively consisting of metallic objects, as only one porcelain is represented there (with #19-F1429C yellow; Table S2). Although a great similarity

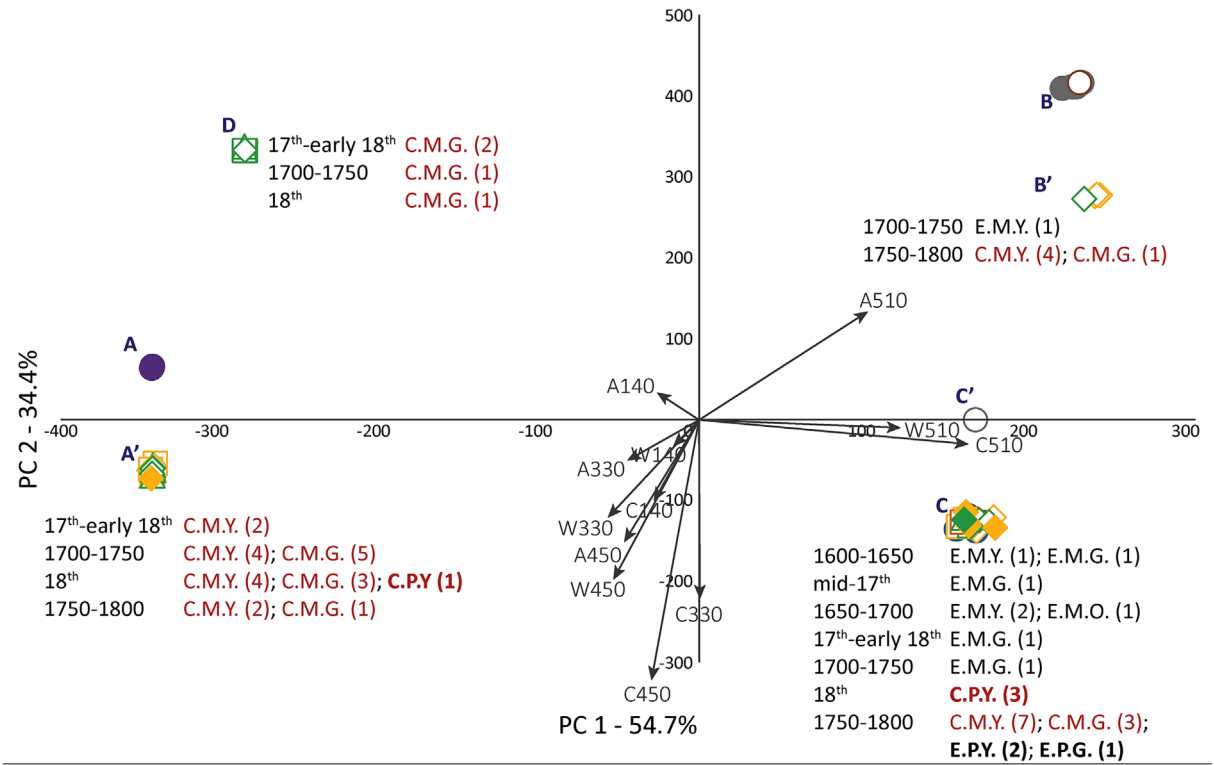

FIGURE 8 PCA diagram of the first and second component calculated from the reference sample, onto which the parameters derived from the decomposition of the enamel spectra are projected (variables are the center of gravity, the width, and the area of the peaks at ~140, 330, 450, and 510 cm^{-1}; centering option: yes; scaling option: no; number of PC max: 20). The vectors show the projection of the variables on the principal components plane. Variables grouped together are positively correlated, while variables positioned on opposite sides of the plot origin (the 510 vs. the 330 for example) are negatively correlated. The further a variable is from the origin, the more it contributes to the components of the factor plane.

can be observed among the Raman signatures of this group, it seems that two groups can be distinguished on the basis of the position of the characteristic Pb peak (T′ Pb^{2+} in Figure 4). Indeed, one group of enamels shows this peak between 125 and 130 cm^{-1}, while another group exhibits it between 132 and 139 cm^{-1}. We note in Figure 4 that all the lead-tin yellow I reference samples appear in the low Raman wavenumber group unlike the lead-tin yellow II samples. Could this be a way to distinguish between the pigments originally used in either form of lead stannate? The question remains open. The other hypothesis is that these differences in the position of this peak would result from differences in the temperatures reached in the firing of these glazes. This was observed for example by Sakellariou et al.[79] by Raman microspectroscopy analysis of a synthesized Naples yellow pigment fired at several temperatures. The Raman wavenumber of the intense characteristic peak decreases with increasing firing temperature, 134 cm^{-1} for the pigment fired at 800°C versus 124 cm^{-1} for the same pigment fired at 1,100°C. Since we are dealing here with comparable conditions and analysis parameters—several studies having shown that the position of the T'_{Pb} band can also depend on the excitation laser wavelength (or the procedure) used[95]—we could then assume that the enamels showing this band at the lower Raman shifts would have been fired at higher temperatures than those showing the same peak at higher ones.

Since, in the vast majority of cases, the enamels analyzed on the same object have their Raman signatures belonging to only one of these subgroups, we checked if there was a correlation between these two subgroups and the manufacturing workshops. We find that this is not the case for two of the three workshops concerned here. Indeed, two objects come from Jingdezhen and two others from the Imperial Palace workshops, and they are respectively distributed in each of the two subgroups. Only the three objects from Ganzhou are all in the higher wavenumber group.

Finally, among the enamels featuring the lead-tin yellow, only two of the 22 analyzed show the two main peaks of cassiterite around 630 and 775 cm^{-1}. Considering that this component can be formed by improper firing conditions of enamels containing these lead-tin pigments, for example, by a higher firing temperature,[96] it would seem that the Chinese artisans developed a good mastery of this production technique (Figures 8 and 10: Groups A and A′).

5.2 | Naples Yellow *stricto* sensu

The reason that leads us to consider the signature group of glazes B′ "neighbors" of the reference Group B is that, based on the variables used, only the presence or absence of the band at ~330 cm^{-1} differentiates them (Figure 8), which is probably linked to a change in symmetry of the structure. An increase of that band can be observed in lead antimonate yellows when there is a substitution of Sb with Si,[95] thus leading to a modification of the Sb-O and Pb ion vibrational modes.[39,49] Since Group B includes only "pure" lead antimonate references, it is normal to not find this band, unlike Group B′ enamels whose manufacture results from the association of a silicate mixture (*corpo*) with a coloring mixture (*anima*),[1,6,99,100] here potentially $Pb_2Sb_2O_7$. In the case of enamels, it is probably one of the components of the silicate mixture (i.e., Fe, K, and Si) that entered into the pyrochlore structure during the firing step and thus modified the Raman signature of the lead antimonate. Similarly, we also find this band at ~330 cm^{-1} among the samples of Group C that present lead antimonates doped with other metals (Sn, Zn, or Fe), clearly illustrating here a substitution of Sb with, for example, Sn or Fe, as it has already been largely observed.[39,49,71,95,101,102] Therefore, the samples of enamels in Group B′ correspond to those whose production of the yellow and green color was most likely based on the use of the Naples yellow pigment ($Pb_2Sb_2O_{7-\delta}$), transformed or not as *frit*, before its addition to the silicate mixture (*corpo*).

Six enamels feature Naples Yellow pigment applied on three different objects. These are a watch manufactured in Paris between 1735 and 1750 (OA8338) and two Chinese metal wares produced in the workshop of the Imperial Palace during the third quarter of the 18th century (F1467 and F1501). We thus observe here that the use of Naples Yellow pigment concerns productions of outstanding metal objects after 1735 (Figures 8 and 10: Groups B and B′).

5.3 | Complex lead antimonate yellow

Complex lead antimonate are pyrochlores in which antimony could have been substituted with Zn, Sn, or Fe and are grouped together in Group C of Figure 7. On the basis of the variables selected for the PCAs, it should also be recalled that it is not possible to clearly differentiate subclusters of this group, which could have allowed differentiation of one variant from another.

Rosi et al.[39] showed that the Pb mode shifts towards higher wavenumbers in the samples doped with Zn and Sn among the modified Naples Yellow references; the larger shift being for Zn-modified Naples Yellow with values up to 145 cm^{-1} (Figure 4). The values measured for this band among the studied enamels do not exceed 141 cm^{-1}. They range between 125 and 141 cm^{-1}, which

corresponds rather well to the range of values measured for lead antimony iron oxide, lead antimony tin oxide, and lead antimony tin silicon oxide, the latter having the lowest values overall in this range (Figure 4). However, it is frequently reported that a doublet is observed instead of this peak for Sn-modified Naples Yellow, which could be explained by the bimodality in the cell size,[39,101] which is not visually the case with the spectra of the enamels analyzed (Figure 1). However, failing to show clearly two bands, some Raman signatures show a wider band, resulting from the combination of two bands (Figure 1B,C). This larger band is exclusively detected among Raman signatures of Group C enamels, which could suggest the presence of lead antimony tin silicon oxide. Nevertheless, these Raman signatures do not allow us to further characterize the pigments used among the modified Naples yellows. Elemental microanalysis is necessary in this case to complete this information.

Five enamels of this group have already been analyzed by pXRF.[19,21] These are #1-OA6224 green, #2-OA100079 yellow, #5-OA7074 green, and #8-OA8435 green enamels from French watches and the #55-yellow enamel from Chinese porcelain TH457. Tin, antimony, and zinc were measured in the glazes of the French watches, except for OA7074, where only Sn and Sb were detected, as in the case of the TH457 glaze. Fe was detected in these five enamels. Thus, in the first three cases, we could assume the use of a Naples Yellow pyrochlore of mixed Sb-Sn-Zn-(Fe) composition, while the two glazes without Zn would illustrate more the use of a Sn-modified Naples Yellow.

In total, 24 of the enamels analyzed show these complex forms of Naples Yellow. They represent 12 objects, including seven European metal watches from the 17th and first half of the 18th century and the two French porcelains of the corpus dated from the second half of the 18th. These are all the European objects in the corpus, except for watch OA8338—the latest—whose enamel contains lead stannate yellow. The three other objects in this group correspond to the two Chinese porcelains of the corpus and one Chinese metalware, all dated to the second third-late 18th century. This fit well with the use of ingredients imported from Europe (Figures 8 and 10: Group C).

5.4 | Unidentified pigment

Four enamels feature an unidentified pigment whose Raman signature show the strong T'_{Pb} at ~130 cm^{-1} as well as that of the band around 330 cm^{-1} (Figure 8: Group D). It concerns only green enamels applied on three of the Chinese metal wares of the study. It is interesting to note that the spectra of the four enamels show important signatures of the silicate matrix (Figure 9), so that the observation of the peaks around 450 and 510 cm^{-1} is made complicated by the naked eye. Furthermore, we note that the other glazes analyzed on the three objects concerned—F1448C, F1735C, and R957—are all of the lead-tin type, whose spectra therefore show the peak around 450 cm^{-1}. These four samples illustrate the need to perform precise X-ray micro-diffraction and elemental analyze (and/or Transmission Electron Microscopy) to determine the nature of the phases/pigments present. To obtain the most accurate results possible, it would be necessary to carry out measurements on microsamples (Figures 8 and 10: Groups A and A′).

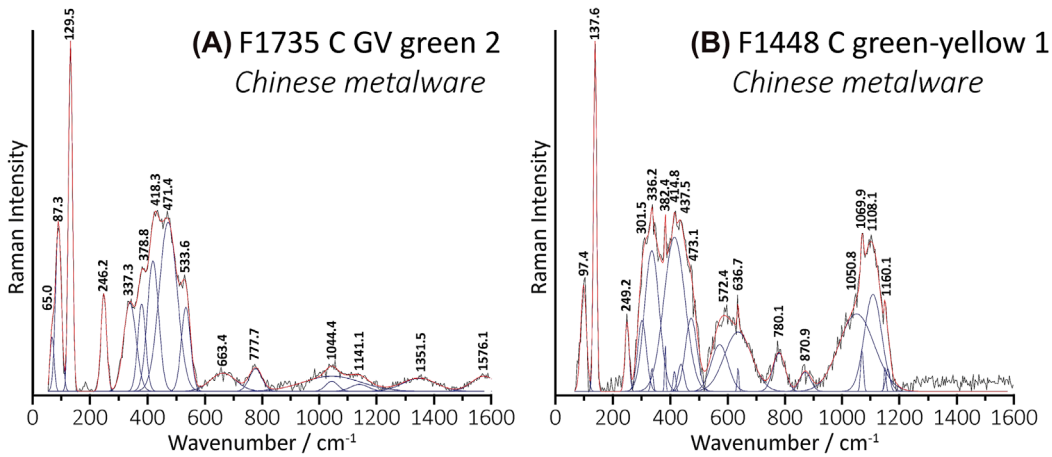

FIGURE 9 Representative spectra of Raman signatures for two green enamels on Chinese metalware (A and B), which belong to PCA's Group D of Figure 8. The decomposition were made after subtracting a baseline and using a Lorentzian shape for thin peaks, a Gaussian shape for wide peaks, and minimizing the number of bands. In both cases, a peak is observed before the T'_{Pb} one.

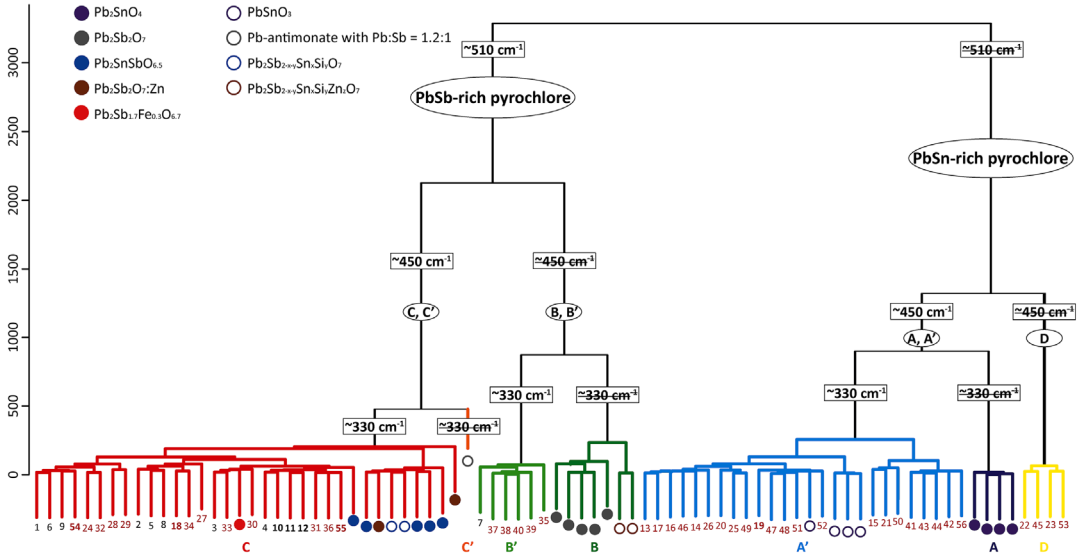

FIGURE 10 Hierarchical clustering using the Euclidian distance and the Ward aggregation rule on the data from spectra decomposition of the studied objects and of the ones from the literature (variables are the center of gravity, the width, and the area of the peaks at ~140, 330, 450, and 510 cm^{-1}; scaling option: no; choice of cluster number: 4). Codes of the samples, id. number (bottom line), are as follow: black for European objects, red for Chinese ones, bold for porcelains, and standard for metalwares.

6 | TRANSFER OF TECHNOLOGY FROM EUROPE TO CHINA

The construction of groups of enamels by pigment category is of course in line with the results and hypotheses already published concerning this corpus.[17,19–23,100]

The painted enamel technology was introduced into China from Europe during the end of the reign of Emperor Kangxi (1662–1722) and was also accompanied by the importation of European coloring ingredients such as the modified lead-antinomy pigment—Pb-Sb-Sn: Zn, Fe, Si—which had principally been used on metal wares in Europe,[103,104] as evidenced by its detection on all the European objects of our corpus, except for the late watch OA8338 (Table S2). This finding is supported not only by analyses—the earliest yellow and green paint enamels applied on Chinese porcelain dating from the Kangxi period were colored with this modified lead-antinomy pigment[12,105,106]—but also by historical sources.[15,30,31,35,107,108] For instance, in a 1714 letter to Pope Clement XI from Italian missionaries sent to the court of the Kangxi Emperor, they asked Rome to send antimony, enamels, and a particular variety of aventurine glass as gifts to the Chinese Court.[107] According to Bellemare,[108] "it is thus possible that the colourant was introduced to the overglaze enamelling palette in the final decade of the Kangxi emperor's reign. This would explain the mention in 1735 by Tang Ying that the Jingdezhen workshops were producing 'Western yellow ware, a new creation of this dynasty'."

Among the samples of our corpus, we find this pigment in all the yellow decorated Chinese objects—mainly porcelains—of the Qianlong period (1736–1795). Concerning metal wares, yellow and green enamels of a 16th century Chinese *cloisonné* vessel (id. number: 23604)[109] and of the metalware F1467 of the present corpus, which features painted and *cloisonné* enamels and whose yellow and green colored enamels, all three types of yellow pigments were detected (see Table S2). Unlike what is reported by Miao et al.,[105] complex Naples Yellow is used in the overglaze enamel technique beyond the early Qianlong period. Not only do we find it on porcelains from this period[21,27] but the Pb-Sb-Sn triple oxide yellow (and green) pigment also seems to have been used until the mid-19th century. However, its usage became less frequent, as it was progressively replaced by the lead-tin yellow pigment.

The first use of "pure" lead-tin yellow in Asia is evidenced for a *Kan'ei* period porcelain (Japan, 1624–1648) made under the guidance of Portuguese Jesuits that established a school (the *Seminario*) teaching the European techniques of painting and enameling.[80,110] In China the "pure" lead-tin yellow start to be used during Wanli reign (1572–1620, Ming Dynasty) on enameled porcelain[109,111] and *cloisonné* metal wares.[109] The question regarding the link between this use in China and the introduction of the technique at the same time in Japan by European missionaries remain open. It is established that Chinese craftsmen from Macau attend the *Seminario*.

For the earliest periods covered by our corpus, this pigment is present on a Chinese metal object with *cloisonné* decoration—F1448C—from the Kangxi period, as well as on two metallic objects with enamel painted decoration—F1341C and R957—from the reign of Emperor Yongzheng (1723–1735) (Table S2). Analyses carried out so far on Chinese enamels attest to the use of this pigment in overglaze porcelain enamels only from the Yongzheng reign period onwards.[27,105,106] It is reported in the *Imperial Workshops Archives* that, in 1728, the Imperial workshops at Beijing sent enamel colors for porcelain to Jingdezhen and that, in 1729, Jingdezhen sent back to the Imperials workshops enamel colors that they created, among which featured the yellow and green ones.[104,112,113] As Chinese workshops were no longer dependent on imported products for the production of yellow and green porcelain enamels,[114] this pigment seems to become more widely used than the antimony-based one from the Qianlong period onwards. Indeed, it is widely used in yellow and green enamels painted on porcelains,[20,21,103,105,114–116] and still on metal wares featuring painted decoration technique[20,23,36] and *cloisonné* one[20,23,117] (Table S2).

Finally, the Naples Yellow pigment *stricto* sensu ($Pb_2Sb_2O_7$) appears later in the productions in question, as it is detected in the enamel of a French watch dated to 1735–1750 and in enamels of two Chinese objects with *cloisonné* enamel decoration—F1467 and F1501C—dated to the third quarter of the 18th century. These dates are earlier than the date from which this pigment is attested by other groups in Chinese overglaze porcelains manufactured in Jingdezhen, that is, around 1911.[105]

7 | CONCLUSIONS

Our study highlights the value of using parameters derived from spectral decompositions of Raman spectra in PCAs to discriminate structural variations in pigments present in a glassy matrix. Previous work on silicate matrices alone showed that for them too, it was necessary to extract spectroscopic parameters[29] in order to classify them on the basis of their Raman signatures. The dataset is characterized by the following features: on-site measurements with a mobile instrument produce spectra with variable backgrounds from one point to another; the variability in the relative intensities of the Raman signals of the different phases present leads to masking of the less intense ones; the compounds of interest are complex solid solutions that are still poorly documented and for which crystallographic and spectroscopic data are lacking.

We observe comparable efficiency between PCA and spectroscopic parameter comparison plots in identifying different yellow pigment groups. PCA facilitates completeness and identification of the most relevant parameters for highlighting groups (with phases not predicted a priori). Indeed, the multivariate approaches used have the advantage of not requiring prior knowledge of all the compounds present and their vibrational signatures. This is particularly the case when, as has been pointed out, the solid solutions under consideration are complex and non-referenced poles are highlighted (in this case the A and A′ groups). Furthermore, the proposed approaches do not require a detailed vibrational study of the spectral signatures if the literature offers reliable reference spectra of all phases. For this purpose, software for extracting data from published spectra (or their availability) is indispensable.

The dendrogram from the hierarchical cluster analysis in Figure 10 summarizes the different types of "Naples yellows" sensu *latu* observed in the enamels. The modified lead antimony yellow and the lead antimony/Naples Yellow *stricto* sensu are characterized by the observation of the band around 510 cm^{-1} related to the Sb-O bond modes. The complex lead-antimony yellow pigment, sometimes referred in the literature as lead-antimony-tin triple oxide, form a group of pigments already well known in Europe during the 17th century, especially for the production of yellow and green enamels painted on metal ware. Its introduction into Chinese porcelain production correlates with the development of the painted enamel technique introduced at the court of the Kangxi Emperor by European missionaries. From the examination of our corpus, this pigment, first imported from Europe, was initially only used in painted enamels on Chinese porcelain and was then also applied on metal from the period of the reign of Emperor Yongzheng. The Naples Yellow pigment *stricto* sensu, on the other hand, seems to have been only used in Chinese and European enamels only later, probably towards the end of the reign of the Qianlong Emperor.

A third type of pigment identified corresponds to the lead-tin yellow. Although known in two forms in painting, lead-tin yellow I (Pb_2SnO_4) and II ($PbSn_{1-x}Si_xO_3$), only type II has been identified so far in Chinese enamels. Initially used in the Chinese production of glass and metal objects decorated according to the *cloisonné* technique, this pigment, whose use in painted enamels on porcelain seems to have been used in the workshops of Jingdezhen, will be more and more used in the production of Chinese enamels, until it almost supplanted the pigment of modified lead-antimony type. Further research is needed to expand the corpus of objects studied that were produced in Europe and Asia, in order to further clarify the history of technological developments and transfers between these two regions.

Raman spectroscopy offers a flexible, mobile and non-invasive analytical approach to characterize the phases that color enamels. However, given the complexity of the solid solutions represented by these yellow pigments, some complementary measurements involving at the micro-scale fine structural characterization (X-ray diffraction, electron imaging, or diffraction) and elemental characterization are still required to clarify the relationships between ancient technologies and the objects recovered.

ORCID

Jacques Burlot https://orcid.org/0000-0002-6451-1788
Divine Vangu https://orcid.org/0009-0004-6474-0304
Ludovic Bellot-Gurlet https://orcid.org/0000-0002-7995-6261
Philippe Colomban https://orcid.org/0000-0001-6099-5423

REFERENCES

[1] P. Colomban, G. Sagon, X. Faurel, *J. Raman Spectrosc.* **2001**, *32*, 351.
[2] R. E. M. Hedges, *Archaeometry* **1976**, *18*, 209.
[3] I. N. M. Wainwright, J. M. Taylor, R. D. Harley, in *Artist' Pigments: A Handbook of Their History and Characteristics*, (Ed: R. L. Feller) Vol. 1, National Gallery of Art, Archetype Publications, Washington, London **1986**, 219.
[4] B. Kırmızı, E. H. Göktürk, P. Colomban, *Archaeometry* **2015**, *57*, 476.
[5] F. Brisse, D. J. Stewart, V. Seidl, O. Knop, *Can. J. Chem.* **1972**, *50*, 3648.
[6] E. Neri, C. Morvan, P. Colomban, M. F. Guerra, V. Prigent, *Ceram. Int.* **2016**, *42*, 18859.
[7] P. Ricciardi, P. Colomban, V. Milande, *J. Raman Spectrosc.* **2008**, *39*, 1113.
[8] J. Dik, E. Hermens, R. Peschar, H. Schenk, *Archaeometry* **2005**, *47*, 593.
[9] D. Hradil, T. Grygar, J. Hradilová, P. Bezdička, V. Grűnwaldová, I. Fogaš, C. Miliani, *J. Cult. Herit.* **2007**, *8*, 377.
[10] U. Santamaria, G. Agresti, C. Pelosi, in *Fatto d'Archimia. Los Pigmentos Artificiales en las Técnicas Pictóricas*, (Eds: M. del Egido, S. Kroustallis), Secretaría General Técnica; Subdirección General de Publicaciones, Información y Documentación, Madrid **2012**, 145.
[11] R. A. Epler, D. R. Epler, *Glazes and Glass Coatings*, The American Ceramic Society, Westerville **2000**.
[12] P. Colomban, A.-T. Ngo, N. Fournery, *Heritage* **2022**, *5*, 233.
[13] P. Colomban, in *Modern Methods for Analysing Archaeological and Historical Glass*, 1st ed. (Ed: K. Janssens), John Wiley and Sons Ltd, London **2012**, 275.
[14] P. Colomban, O. Paulsen, *J. Am. Ceram. Soc.* **2005**, *88*, 390.
[15] P. Colomban, Y. Zhang, B. Zhao, *Ceram. Int.* **2017**, *43*, 12079.
[16] P. Colomban, F. Ambrosi, A.-T. Ngo, T.-A. Lu, X.-L. Feng, S. Chen, C.-L. Choi, *Ceram. Int.* **2017**, *43*, 14244.
[17] P. Colomban, T.-A. Lu, V. Milande, *Ceram. Int.* **2018**, *44*, 9018.
[18] P. Colomban, M. Maggetti, A. d'Albis, *J. Eur. Ceram. Soc.* **2018**, *38*, 5228.
[19] P. Colomban, B. Kırmızı, C. Gougeon, M. Gironda, C. Cardinal, *J. Cult. Herit.* **2020**, *44*, 1.
[20] P. Colomban, B. Kırmızı, B. Zhao, J.-B. Clais, Y. Yang, V. Droguet, *Coatings* **2020**, *10*, 471.
[21] P. Colomban, B. Kırmızı, B. Zhao, J.-B. Clais, Y. Yang, V. Droguet, *Heritage* **2020**, *3*, 915.
[22] P. Colomban, M. Gironda, H. G. M. Edwards, V. Mesqui, *J. Raman Spectrosc.* **2021**, *52*, 2246.
[23] P. Colomban, M. Gironda, D. Vangu, B. Kırmızı, B. Zhao, V. Cochet, *Materials* **2021**, *14*, 7434.
[24] P. Colomban, *Orientations* **2022**, *53*, 92.
[25] P. Colomban, *Materials* **2022**, *15*, 3158.
[26] P. Colomban, *L'Actualité Chim.* **2022**, *476*, 8.
[27] P. Colomban, M. Gironda, G. Simsek Franci, P. d'Abrigeon, *Materials* **2022**, *15*, 5747.
[28] P. Colomban, A.-T. Ngo, H. G. M. Edwards, L. C. Prinsloo, L. V. Esterhuizen, *Ceram. Int.* **2022**, *48*, 1673.
[29] P. Colomban, A. Tournié, *J. Cult. Herit.* **2007**, *8*, 242.
[30] C.-F. Shih, *Radiant Luminance: The Painted Enamelware of the Qing Imperial Court*, The National Palace Museum of Taipei, Taipei, Taiwan **2012**.
[31] C.-F. Shih, *Natl. Palace Mus. Res. Q.* **2017**, *24*, 45.
[32] B. Zhao, G. Y. Wang, I. Biron, P. Colomban, L. Hilaire-Pérez, *CNRS En Chine Bull.* **2016**, *21*, 20.
[33] B. Zhao, F. Simon, in *Des Arts Diplomatiques. Échanges de Présents Entre la Chine et l'Europe, XVIIe-XVIIIe Siècles*, (Eds: B. Zhao, I. Landry-Deron, F. Simon), Presses Universitaires de Vincennes, Vincennes **2019** 5.
[34] B. Zhao, *Orientations* **2022**, *53*, 78.
[35] B. Zhao, *Orientations* **2022**, *53*, 80.
[36] H. Liu, H. Wang, P. Duan, H. Gao, R. Zhang, L. Qu, *Herit. Sci.* **2022**, *10*, 132.
[37] S. A. Ivanov, V. E. Zavodnik, *Kristallografiya* **1990**, *35*, 842.
[38] R. J. H. Clark, L. Cridland, B. M. Kariuki, K. D. M. Harris, R. Withnall, *J. Chem. Soc., Dalton Trans.* **1995**, 2577.
[39] F. Rosi, V. Manuali, C. Miliani, B. G. Brunetti, A. Sgamellotti, T. Grygar, D. Hradil, *J. Raman Spectrosc.* **2009**, *40*, 107.
[40] G. Natta, M. Baccaredda, *Z. Für Krist.* **1933**, *85*, 271.
[41] U. Hålenius, F. Bosi, *Mineral. Mag.* **2013**, *77*, 2931.
[42] C. Cascales, J. A. Alonso, I. Rasines, *J. Mater. Sci. Lett.* **1986**, *5*, 675.
[43] H. E. Swanson, H. F. McMurdie, M. C. Morris, E. H. Evans, B. Paretzkin, *Standard X-Ray Diffraction Powder Patterns—Section 10—Data for 84 Substances*, Washington D.C, Institute for Materials Research **1972**.
[44] J. R. Gavarri, J. P. Vigouroux, G. Calvarin, A. W. Hewat, *J. Solid State Chem.* **1981**, *36*, 81.
[45] D. Spahr, M. Stękiel, D. Zimmer, L. Bayarjargal, K. Bunk, W. Morgenroth, V. Milman, K. Refson, D. Jochym, P. J. P. Byrne, B. Winkler, *Acta Crystallogr. Sect. B Struct. Sci. Cryst. Eng. Mater.* **2020**, *76*, 979.
[46] H. P. Rooksby, *Phys. Chem. Glasses* **1964**, *5*, 20.
[47] I. Morgenstern Badarau, M. A. Michel, *Ann. Chim.* **1971**, *6*, 109.
[48] C. Cascales, I. Rasines, P. G. Casado, J. Vega, *Mater. Res. Bull.* **1985**, *20*, 1359.

[49] L. Cartechini, F. Rosi, C. Miliani, F. D'Acapito, B. G. Brunetti, A. Sgamellotti, *J. Anal. At. Spectrom.* **2011**, *26*, 2500.

[50] F. Alloteau, O. Majérus, F. Gerony, A. Bouquillon, C. Doublet, H. Gries, A. Fügert, A. Thomas, G. Wallez, *Minerals* **2022**, *12*, 311.

[51] C. Pelosi, G. Agresti, U. Santamaria, E. Mattei, *E-Preserv. Sci.* **2010**, *7*, 108.

[52] E. Gliozzo, C. Ionescu, *Archaeol. Anthropol. Sci.* **2022**, *14*, 17.

[53] M. T. Vandenborre, E. Husson, H. Brusset, A. de Cerez, *Spectrochim. Acta Part Mol. Spectrosc.* **1980**, *36*, 1045.

[54] M. T. Vandenborre, E. Husson, *Mater. Res. Bull.* **1982**, *17*, 1289.

[55] M. T. Vandenborre, E. Husson, *J. Solid State Chem.* **1984**, *53*, 253.

[56] B. Mihailova, M. Gospodinov, B. Güttler, R. Stosch, U. Bismayer, *J. Phys.: Condens. Matter* **2007**, *19*, 275205.

[57] H. Kühn, in *Artist' Pigments: A Handbook of Their History and Characteristics*, (Ed: R. Ashok) Vol. 2, National Gallery of Art, Archetype Publications, Washington, London **1993** 83.

[58] A. E. Werner, M. Bimson, *Archaeologia* **1967**, *101*, 16.

[59] J. Henderson, in *Hengistbury Head Dorset, Volume 1: The Prehistoric and Roman Settlement 3500 BC–AD 500*, (Ed: B. Cunliffe), Oxford University Committee for Archaeology, Oxford **1987**, 160 180–186.

[60] M. V. Talanov, V. M. Talanov, *Chem. Mater.* **2021**, *33*, 2706.

[61] Y.-J. Hsiao, Y.-H. Chang, T.-H. Fang, Y.-S. Chang, Y.-L. Chai, *J. Alloys Compd.* **2007**, *430*, 313.

[62] F. S. Galasso, *Structure, Properties and Preparation of Perovskite-Type Compounds*, Pergamon Press, Elmsford, New York **1969**.

[63] H. Yokokawa, N. Sakai, T. Kawada, M. Dokiya, *J. Solid State Chem.* **1991**, *94*, 106.

[64] A. S. Bhalla, R. Guo, R. Roy, *Mater. Res. Innovations* **2000**, *4*, 3.

[65] A. Slodczyk, P. Colomban, M. Pham-Thi, *J. Phys. Chem. Solids* **2008**, *69*, 2503.

[66] A. Slodczyk, P. Colomban, *Materials* **2010**, *3*, 5007.

[67] T. Siritanon, A. W. Sleight, M. A. Subramanian, *Mater. Res. Bull.* **2011**, *46*, 2494.

[68] M. J. Winiarski, T. M. McQueen, *J. Solid State Chem.* **2019**, *278*, 120898.

[69] A. Marchetti, R. Saniz, D. Krishnan, L. Rabbachin, G. Nuyts, S. de Meyer, J. Verbeeck, K. Janssens, C. Pelosi, D. Lamoen, B. Partoens, K. de Wael, *Chem. Mater.* **2020**, *32*, 2863.

[70] P. Ricciardi, P. Colomban, A. Tournié, M. Macchiarola, N. Ayed, *J. Archaeol. Sci.* **2009**, *36*, 2551.

[71] C. Sandalinas, S. Ruiz-Moreno, *Stud. Conserv.* **2004**, *49*, 41.

[72] WebPlotDigitizer, https://automeris.io/WebPlotDigitizer/, (accessed 22 November 2022).

[73] P. Colomban, *J. Cult. Herit.* **2008**, *9*, e55.

[74] M. C. Caggiani, P. Colomban, C. Valotteau, A. Mangone, P. Cambon, *Anal. Methods* **2013**, *5*, 4345.

[75] Galaxy/ChemFlow 20.05, https://vm-chemflow-francegrille.eu/, (accessed 22 November 2022).

[76] J.-M. Roger, J.-C. Boulet, M. Zeaiter, D. N. Rutledge, in *Comprehensive Chemometrics: Chemical and Biochemical Data Analysis*, 2nd ed. (Eds: S. Brown, R. Tauler, B. Walczak) Vol. 3, Elsevier, Amsterdam **2020**, 1.

[77] R. J. Barnes, M. S. Dhanoa, S. J. Lister, *Appl. Spectrosc.* **1989**, *43*, 772.

[78] B. Kırmızı, P. Colomban, M. Blanc, *J. Raman Spectrosc.* **2010**, *41*, 1240.

[79] K. Sakellariou, C. Miliani, A. Morresi, M. Ombelli, *J. Raman Spectrosc.* **2004**, *35*, 61.

[80] R. Montanari, N. Murakami, P. Colomban, M. F. Alberghina, C. Pelosi, S. Schiavone, *Herit. Sci.* **2020**, *8*, 48.

[81] B. Mihailova, S. Stoyanov, V. Gaydarov, M. Gospodinov, L. Konstantinov, *Solid State Commun.* **1997**, *103*, 623.

[82] P. Bourson, G. Simon, D. Chapron, N. Kokanyan, P. Colomban, in *Spectroscopies Vibrationnelles: Théorie, Aspects Pratiques et Applications*, (Ed: G. Simon), Editions des Archives Contemporaines, Paris **2020** 109.

[83] C. Chemarin, N. Rosman, T. Pagnier, G. Lucazeau, *J. Solid State Chem.* **2000**, *149*, 298.

[84] A. Slodczyk, P. Daniel, A. Kania, *Phys. Rev. B* **2008**, *77*, 184114.

[85] J. S. Bae, I.-S. Yang, J. S. Lee, T. W. Noh, T. Takeda, R. Kanno, *Vib. Spectrosc.* **2006**, *42*, 284.

[86] S. Saha, S. Prusty, S. Singh, R. Suryanarayanan, A. Revcolevschi, A. K. Sood, *J. Solid State Chem.* **2011**, *184*, 2204.

[87] K. Ueda, R. Kaneko, A. Subedi, M. Minola, B. J. Kim, J. Fujioka, Y. Tokura, B. Keimer, *Phys. Rev. B* **2019**, *100*, 115157.

[88] J. S. Bae, I.-S. Yang, J. S. Lee, T. W. Noh, T. Takeda, R. Kanno, *Phys. Rev. B* **2006**, *73*, 052301.

[89] H. Haeuseler, *Spectrochim. Acta Part Mol. Spectrosc.* **1981**, *37*, 487.

[90] P. Colomban, B. Kırmızı, G. Simsek Franci, *Minerals* **2021**, *11*, 633.

[91] P. Colomban, *J. Non-Cryst. Solids* **2003**, *323*, 180.

[92] V. Labet, P. Colomban, *J. Non-Cryst. Solids* **2013**, *370*, 10.

[93] J. Burlot, D. Vangu, L. Bellot-Gurlet, P. Colomban, *J. Raman Spectrosc.*, submitted.

[94] B. Manoun, M. Azdouz, M. Azrour, R. Essehli, S. Benmokhtar, L. el Ammari, A. Ezzahi, A. Ider, P. Lazor, *J. Mol. Struct.* **2011**, *986*, 1.

[95] V. Antušková, R. Šefců, P. Šulcová, Ž. Dohnalová, J. Luxová, M. Bajeux Kmoníčková, I. Turková, M. Kotrlý, *J. Raman Spectrosc.* **2022**, *54*, 171.

[96] R. Šefců, Š. Chlumská, A. Hostašová, *Herit. Sci.* **2015**, *3*, 16.

[97] P. Colomban, in *Encyclopedia of Glass Science, Technology, History, and Culture*, (Ed: P. Richet), J. Wiley & Sons Inc., New York **2020**.

[98] P. Colomban, in *Conservation Science—Heritage Materials*, 2nd ed. (Eds: P. Garside, E. Richarson), The Royal Society of Chemistry, Cambridge **2019**, 200.

[99] A. d'Albis, *Traité de la Porcelaine de Sèvres*, Faton, Dijon **2003**.

[100] P. Colomban, G. Simsek Franci, J. Burlot, X. Gallet, B. Zhao, J.-B. Clais, *Ceramics* **2023**, *6*, 447.

[101] F. Rosi, V. Manuali, T. Grygar, P. Bezdicka, B. G. Brunetti, A. Sgamellotti, L. Burgio, C. Seccaroni, C. Miliani, *J. Raman Spectrosc.* **2011**, *42*, 407.

[102] C. Sandalinas, S. Ruiz-Moreno, A. López-Gil, J. Miralles, *J. Raman Spectrosc.* **2006**, *37*, 1146.

[103] H. Duan, X. Zhang, B. Kang, G. Wang, L. Qu, Y. Lei, *Stud. Conserv.* **2019**, *64*, 311.
[104] C.-F. Shih, in *The RA Collection of Chinese Enamelled Copper. A Collector's Vision*, (Eds: M. A. P. de Matos, A. Moás, C.-F. Shih) Vol. V, Jorge Welsh Research & Publishing, London **2021**, 28.
[105] J. Miao, B. Yang, D. Mu, *Archaeometry* **2010**, *52*, 146.
[106] J. Hou, Y. Ding, H. Li, C. Lü, *J. Gugong Stud.* **2018**, *19*, 210.
[107] E. B. Curtis, in *Des Arts Diplomatiques. Les Cadeaux Diplomatiques Entre la Chine et l'Europe aux XVIIe-XVIIIe Siècles. Pratiques et Enjeux*, (Eds: B. Zhao, I. Landry-Deron, F. Simon), Presses Universitaires de Vincennes, Vincennes **2019**, 29.
[108] J. Bellemare, *J. Glass Stud.* **2022**, *64*, 147.
[109] B. Kırmızı, P. Colomban, B. Quette, *J. Raman Spectrosc.* **2010**, *41*, 780.
[110] R. Montanari, M. F. Alberghina, A. C. Municchia, E. Massa, A. Pelagotti, C. Pelosi, S. Schiavone, A. Sodo, *J. Cult. Herit.* **2018**, *32*, 232.
[111] N. Wood, *Chinese Glazes: Their Origins, Chemistry, and Recreation Chinese Glazes: Their Origins, Chemistry, and Recreation*, A&C Black, London **1999**.
[112] P. Mills, R. Kerr, *Stud. Conserv.* **2000**, *45*, 21.
[113] H. Tang, 'The colours of each piece': Production and consumption of Chinese enamelled porcelain, c.1728–c.1780, Unpublished Ph.D. Thesis, University of Warwick, Department of History, **2017**.
[114] D. E. Norris, *J. Inst. Conserv.* **2015**, *38*, 145.
[115] J. van Pevenage, D. Lauwers, D. Herremans, E. Verhaeven, B. Vekemans, W. de Clercq, L. Vincze, L. Moens, P. Vandenabeele, *Anal. Methods* **2014**, *6*, 387.
[116] Y. Li, P. Sciau, J. Zhu, L. Ji, Y. Shan, G. Song, *Microsc. Res. Tech.* **2021**, *84*, 1106.
[117] Y. Su, L. Qu, H. Duan, N. Tarcea, A. Shen, J. Popp, J. Hu, *Spectrochim. Acta. A. Mol. Biomol. Spectrosc.* **2016**, *153*, 165.

SUPPORTING INFORMATION

Additional supporting information can be found online in the Supporting Information section at the end of this article.

How to cite this article: J. Burlot, D. Vangu, L. Bellot-Gurlet, P. Colomban, *J Raman Spectrosc* **2023**, 1. https://doi.org/10.1002/jrs.6600